CARBON 70 (2014) 1–21

Available at www.sciencedirect.com

ScienceDirect

journal homepage: www.elsevier.com/locate/carbon

Review

Mechanisms of graphene growth by chemical vapour deposition on transition metals

Choon-Ming Seah [a], Siang-Piao Chai [b], Abdul Rahman Mohamed [a,*]

[a] School of Chemical Engineering, Engineering Campus, Universiti Sains Malaysia, 14300 NibongTebal, SeberangPerai Selatan, P. Pinang, Malaysia

[b] Chemical Engineering Discipline, School of Engineering, Monash University, Jalan Lagoon Selatan, 46150 Bandar Sunway, Selangor, Malaysia

ARTICLE INFO

Article history:
Received 29 July 2013
Accepted 23 December 2013
Available online 3 January 2014

ABSTRACT

Graphene has become the focus of research recently due to its properties. Various methods have been proposed for the synthesis of graphene, and chemical vapour deposition (CVD) appears to be the most promising route for synthesising large-area graphene. Use of Ru, Ir, Ni, or Co lead to a segregation growth procedure, in which carbon dissolves into the bulk metals at a high temperature and segregates to form graphene after reaching the carbon saturation, and the graphene expand with carpet growth mode. For Cu catalyst, the formation of graphene can be explained by the surface growth model, in which carbon aggregates at the surface of Cu to form graphene. Graphene are formed at different mechanism on different crystalline facets for Pt, Ni and Cu. Meanwhile Ru(0001) and Ir(111) only suitable for graphene formation for respective metals. This review discusses the fundamental mechanisms of the synthesis of graphene from various transition metals under various circumstances through a CVD process and concludes by addressing the challenges involved in large-scale graphene synthesis and the reuse of the catalysts.

© 2013 Elsevier Ltd. All rights reserved.

Contents

1. Introduction . . . 2
2. Chemical vapour deposition . . . 2
3. Catalysts . . . 5
   3.1. Ru . . . 5
   3.2. Ir . . . 8
   3.3. Pt . . . 9
   3.4. Ni . . . 10
   3.5. Cu . . . 11
   3.6. Others . . . 13
4. Future prospects . . . 15

* *Corresponding author:* Fax: +60 594 1013.
E-mail address: chrahman@eng.usm.my (A.R. Mohame).

0008-6223/$ - see front matter © 2013 Elsevier Ltd. All rights reserved.
http://dx.doi.org/10.1016/j.carbon.2013.12.073

5. Summary . . . 15
Acknowledgements . . . 15
References . . . 16

1. Introduction

Graphene is composed of a single layer of sp^2-bonded carbon atoms arranged in a two-dimensional honeycomb crystal lattice either freely suspended form or adhered on any substrate. The lateral dimension of graphene can be in nanoscale or macroscale [1]. Graphene was transformed recently from an "academic" material to an important material that has been the focus of both fundamental and applied scientific studies since 2004, when free-standing graphene was successfully exfoliated mechanically by Novoselov et al. [2]. According to the Mermin–Wagner theorem [3], graphene was thought to be an unstable material due to thermal fluctuations that would prevent this material from existing with long-range crystalline order at finite temperatures [4]. The discovery of the exfoliation method ignited additional interest in research on carbon nanomaterials after 1991, when carbon nanotubes (CNTs) were reported by Professor Sumio Iijima [5].

These outstanding properties of graphene and its multiple applications have attracted a significant number of researchers to look into methods for producing highly crystalline wafer-scale graphene. The Manchester group first reported the "scotch tape" method for exfoliating graphene from highly ordered pyrolytic graphite (HOPG) in 2004 [2]. Their work produced graphene with a perfect crystal structure, as predefined in HOPG. However, the mechanical exfoliation of HOPG is not suitable for mass-producing large-area graphene sheets. Furthermore, the size of the graphene produced by this method is usually on the order of micrometres. Wet chemical exfoliation of graphene can be performed through an ultrasonication treatment of graphite using polymer–organic solvents [6] or organic solvents [7] with a surface energy that matches that of graphene. This approach produces graphene with a smaller size. However, prolonged exposure to sonification may cause structural damage to the graphene.

Graphene can be chemically derived from graphite. Graphene oxide (GO) can be prepared by the Hummers [8], Brodie, or Staudenmaier [9] methods, which are subsequently followed by sonication. GO is dispersable in water. This is attributed to the interaction between the water and the oxygen-containing functionalities introduced to the basal plane of graphene. The hydrophobicity of the graphene is destroyed, and it becomes hydrophilic, which causes the water to readily intercalate between the graphene sheets and disperse them as individual sheets of graphene under mild sonication [10]. The methods to reduce GO to graphene have been reported in [11]. In addition to sonication, GO can also be exfoliated thermally. Under high temperatures and inert conditions, the oxygen will partially oxidise the carbon basal plane of GO to form CO_2 and water. This sudden expansion of gas between the graphene layer would exfoliate the graphite [12]. Other volatile substances, such as ClF_3 [13], are also employed to intercalate graphene sheets; thermal shock is used to volatise the substance and separate the graphene sheets from each other. However, it is difficult for GO to be reduce to pure graphene. The reduction process introduces structural defects into the graphene.

There are two main methods that have been widely used to grow wafer-scale graphene, namely, the epitaxial growth of graphene from SiC and the catalytic chemical vapour deposition (CVD) of carbon precursors. The advantages of epitaxial growth include the ability to produce monolayers graphene in a controllable manner. However, this method has several drawbacks, such as the need for an atomically flat surface covered by a single layer of graphene, which requires advances in SiC substrate preparation and intimate knowledge of graphene nucleation and growth [14]. In addition, the transfer of graphene to another substrate is complicated. Comparatively, CVD is a rather easy approach to obtain graphene with the desired features. CVD is widely known to involve the decomposition of a carbon feedstock, either hydrocarbons or polymers, with the aid of heat and metal catalysts. Various metals, such as Cu, Ni, Pt, Ru, and Ir, have been proven to catalyse the growth of graphene. The number of graphene layers can be controlled by the type and thickness of the catalyst used, whereas the size of the graphene corresponds to the size of the catalyst. This review discusses the fundamental mechanisms of the synthesis of graphene from various transition metals under various circumstances through a CVD process and concludes by addressing the challenges involved in large-scale graphene synthesis and the reuse of the catalysts.

2. Chemical vapour deposition

Generally, the formation of graphene on transition metals through CVD follows a two-step mechanism. The first step is the dilution or incorporation of carbon into the metal, which is better known as dissolution, which is then followed by the formation of a graphene through rapid cooling, also known as segregation. Fig. 1 shows the typical graphene formation by the precipitation/segregation process using CVD. According to Blakely's group [15], they observed the segregation of graphene from a Ni surface, where segregation involves compositional heterogeneity in thermal equilibrium under conditions that correspond to one phase field in the phase diagram, whereas precipitation indicates the inhomogeneity due to the equilibrium phase separation [16]. In a later study by Blakely's group, the authors found that monolayers graphene grew with segregation in the initial stage, followed by precipitation for graphite formation [17]. As shown in Fig. 1, the hydrocarbon that chemisorbs on the metal surface (step 1) dissociates through dehydrogenation (step 2), and the dissolute carbon adatoms will diffuse into the bulk metal (step 3). The chemisorption is facilitated by the empty d-shell of the transition metals, which is ready to serve as an electron

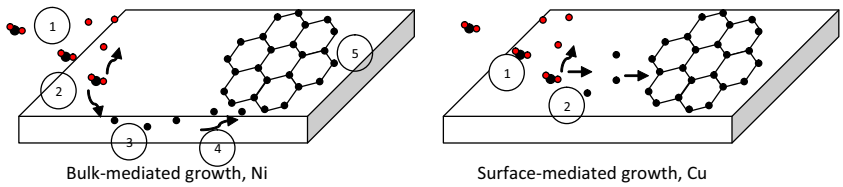


Fig. 1 – Sketch of graphene formation steps on Ni and Cu [19]. (A color version of this figure can be viewed online.)

acceptor. The segregation process will begin when the concentration of carbon adatoms in the bulk metal has achieved the threshold for nucleation or during the cooling process, during which time the carbon solubility in the metal decreases. The excess diluted carbon adatoms diffuse to the surface (step 4), and then the segregation process for graphene formation occurs (step 5). The segregation does not stop until the concentration of carbon in the bulk metal has decreased to equilibrium, even though the supply of hydrocarbon has been switched off [18]. Both the nucleation and equilibrium concentrations are different under different operating conditions. The precipitation/segregation mechanism can be applied to explain graphene formation for most of the transition metals.

The solubility of carbon in Cu is very low. Thus, the chemisorption/deposition or surface growth mechanism better explains the graphene formation mechanism. The growth of graphene would start right after the hydrocarbon dissociation and stop immediately when the supply of hydrocarbon is cut off (steps 1 and 2 in Fig. 1). The detailed growth mechanism for graphene will be further discussed in Section 3.5.

Temperature-Programmed Growth (TPG) is slightly different from CVD in that the hydrocarbon is exposed to the transition metal at room temperature. The empty d-shell of the transition metal enables the adsorption of hydrocarbon, followed by sequential heating to the appropriate temperature for hydrocarbon decomposition and nucleation for graphene formation. The size of graphene grown with TPG was much smaller than the graphene size obtained from CVD, which ranged from a few nanometres to hundreds of nanometres depending on the growth temperature [20].

CVD has been extensively modified to improve its performance for graphene formation. Plasma-enhanced CVD is a feasible approach for large-area graphene synthesis with enhanced growth rates at a lower temperature. The lowest temperature ever recorded for growing graphene was 240 °C [21]. In this method, plasma is generated through radio frequencies [22,23], magnetically enhanced arc discharges [24,25] or microwaves [21,26]. The plasma and metal coupling cause localised rapid heating of the metal catalyst, which reduces the heating time. Moreover, plasma has the ability to remove the native oxide layer and to ensure the uniform nucleation of graphene on the metal substrate [27]. However, plasma-enhanced CVD has several drawbacks, which include the fact that continuous plasma bombardment causes defects in the graphene. Moreover, the resulting graphene has a grain size that is inversely correlated to the intensity of the radicals, which causes a discontinuous graphene sheet with more defects. The fast graphene synthesis in plasma-enhanced CVD also produces amorphous carbon graphene [28]. Woo et al. [29] had reviewed that the quality of graphene is much better under high temperature PECVD rather than low temperature PECVD.

Another controversial aspect of CVD is the use of hydrogen gas (H_2). Some researchers believe that the presence of H_2 in CVD degrades the crystallinity of graphene and slows down the growth rate on the Cu catalyst [30]. H_2 dissociative chemisorption is competing with the dehydrogenation of hydrocarbon by occupying the surface active sites, inhibiting the growth of graphene, and creating point defects on the graphene [19]. The etching power of H_2 on graphene is stronger in the presence of transition metals, which may cause the etching of graphene to form hydrocarbon radicals [31]. The unique growth-limiting property of monolayer graphene on Cu could be destroyed under high H_2 partial pressures [32]. However, there are different views on this topic, some of which suggest that H_2 plays a vital role as an activator of surface-bound carbon and an etching reagent for unorganised or defective graphene edges that will inhibit the graphene growth. Vlassiouk et al. [33] found that graphene could not be grown in the absence of H_2. Under high H_2 partial pressures, H_2 assists in the formation of CH_3 radicals, which are required to grow graphene. Meanwhile, under moderate H_2 partial pressures, the graphene grains formed were irregular in shape. A high H_2 partial pressure caused the formation of more organised hexagonal graphene islands by etching away unstable graphene edges. For other metals, the diffusivity of H in Ni is much lower than that in Cu. The fast recombination and desorption of hydrogen allows the surface of Ni to always be available for hydrocarbons and radicals, facilitating a fast in-diffusion of carbon into Ni [19]. For other transition metals for which the growth of graphene follows the precipitation/segregation process, such as Pt, H_2 has been reported to suppress the extension of minority domains, leaving one millimetre-scale single-crystalline graphene as the dominant domain, which is more difficult to etch with H_2 [34]. Other than that, the working parameter such as temperature, carbon source and pressure are also playing decisive role in determining the overall outcome of as-grown graphene.

Temperature is the main source of energy for the decomposition of carbon precursors and for the activation of a catalyst. For a typical CVD, the temperature in the range of 800–1000 °C is usually employed for most of the catalysts, such as Cu, Ni, Ru and Pt, to grow graphene sheets. The activity of Cu is one of the lowest among the aforementioned catalysts. Cu has a filled 3d shell which is resulting lower carbon solubility and lowers the tendency for adsorbing hydrocarbons (carbon precursor for graphene) onto the Cu surface

[35]. As a consequence, higher temperature is required for graphene to form on Cu. Regmi et al. [36] reported that graphene could be formed at a temperature of below 850 °C through CVD using Cu catalyst but the graphene sheet contained large amount of defects. The quality and the percentage of monolayer graphene formed increased with temperature. According to Li et al. [37], lower temperature favoured the formation of high density and small area graphene; whereas, high temperature formed low density and large area graphene. This was attributed by higher adsorption of hydrocarbon onto the Cu surface that caused denser nucleation at a relatively low temperature [38]. In fact, methane could be decomposed to form graphene at a temperature of as low as 400 °C [39]. Carbon supersaturation was less likely to occur at this temperature and low diffusion energy of carbon atom onto the Cu surface caused the expansion of graphene to be less significant [40]. However, the temperature at 1050 °C, i.e., just below the melting point of the Cu, did not favour the formation of graphene of high crystallinity [41].

According to Liu et al. [42], the high diffusion rate of carbon in the Ni catalyst at a temperature of 1000 °C formed multilayer graphene sheets. At a temperature of 1100 °C, the equilibrium shifted to condensed monolayer state which led to the formation of monolayer graphene on the Ni surface. Meanwhile, above 1150 °C, the solubility of carbon increased exponentially, and lower coverage of graphene was obtained. Odahara et al. [43] observed a similar trend too but the condensed monolayer state was obtained at ~800 °C. On the other hand, at a lower temperature, the characteristics of Ni are different from other transition metals on graphene nucleation. The Ni film forms Ni_2C with a single atom thickness, and this carbide inhibits the growth of graphene. However, disagreement still exists about how the carbide layer will affect the graphene formation as well as its interaction with the graphene. According to Lahiri et al. [44,45], under an ultra-high vacuum condition, three different scenarios can happen: At low temperatures (<460 °C), a single layer of Ni_2C preferentially grows on Ni(1 1 1) after exposing the Ni catalyst to the hydrocarbons. It is believed that the carbide will slowly transform into graphene. For the intermediate temperatures (460–650 °C), the graphene formation follows the segregation/precipitation mechanism. At the temperatures higher than 650 °C, the solubility of carbon increases but still barely below 0.1 wt% at 650 °C, carbon will segregate to graphene during the cooling stage [46]. However, this theory was opposed by Jacobson et al. [47] who failed to observe the Ni_2C. Grüneis et al. [48] also found that the carbide was unable to transform into graphene.

Various temperatures have been reported for graphene nucleation on Pt catalyst [49] Most of the studies showed that that the temperature of ~1000 °C is the most suitable for growing continuous graphene [34,50,51]. An interesting observation is the graphene formed on the Pt appears in different rotations under different temperatures [52]. The temperature to form high quality graphene over Ru catalyst was found to be around 1000 °C [53,54]. The studies of Zhang et al. [55] showed that the high density and small graphene islands were seen all over the Ru surface at low temperature.

Gaseous short chain hydrocarbons, such as methane and ethane, are the most common carbon precursors for the growth of graphene. In the latest study, some researchers found that unsaturated hydrocarbons, such as ethylene and acetylene, could also be used as the carbon precursors for the formation of graphene. It was reported that the growth temperature was significantly reduced to ~650 °C when acetylene was used as the carbon precursor [56]. Furthermore, it was noted that the decomposition temperature of ethylene is relatively low as compared to methane [57]. Acetylene or ethylene is able to attach on the transition metals firmly with its π-bond. It facilitates the dissociation of the hydrocarbon for the formation of graphene sheets [58]. On the other hand, aliphatic alcohols are easier to be handled and stored, less flammable as compared to gaseous hydrocarbons [59]. Monolayer and less defect graphene sheets were obtained when alcohol was used with the Ni catalyst [60]. For both the Ni and Cu catalysts, short chain alcohols were found to form monolayer graphene of high crytallinity with ease [59,60]. A significant breakthrough in the liquid-carbon CVD was reported, where graphene flake was found on the Cu catalyst at the growth temperature of 300 °C using benzene as the carbon precursor [39,61]. Aromatic hydrocarbons were found to have the lower energy barrier for the nucleation of graphene as compared to other gaseous hydrocarbons [39,61]. Other aromatic hydrocarbons such as pyridine [62], hexachlorobenzene [63] and bianthryl [64], as well as the polycyclic aromatic hydrocarbons such as hexabenzocoronene [65] and corroenene [66] required lower temperature to grow the graphene. On the other hand, solid carbon precursors such as amorphous carbon [67], highly oriented pyrolitic graphite (HOPG) [46] and polymers such as poly(methyl methacrylate) (PMMA), high-impact polystyrene, acrylonitrile–butadiene–styrene can form graphene in the presence of the suitable catalysts [68–70]. The recent finding showed that food, solid waste and insect parts can also be used as the source of carbon to grow pure graphene [71,72].

Graphene growth pressure is another issue that is widely debated by researchers. Atmospheric pressure CVD would allow the saturation of carbon on metal catalyst faster, but the carbon precipitation process at the later stage is harder to control [44]. The variation of pressure is giving more significant effect when Cu serves as the catalyst. The sputtered Cu film could be dewetted under low pressure CVD [73]. Besides that, hydrocarbon is difficult to be decomposed under high vacuum condition [74]. The shape of the graphene flake formed is also varied with respect to the pressure employed during the graphene synthesis. The self-limiting monolayer graphene formation over the Cu catalyst was only achieved in a very low pressure CVD. Under ambient pressure, non-uniform multilayer graphene was obtained, caused by the low mass transport rate of carbon [75]. It is known that the coverage of graphene on the catalyst and layer of the graphene sheets increase with the growth pressure. It has been reported that the rate-limiting-step for graphene formation in an atmospheric pressure CVD is the mass transport of hydrocarbon from bulk to the surface of the catalyst. On the contrary, the surface reaction is the rate-limiting-step in a low pressure or ultra high vacuum CVD [32]. Besides that, the activation energy of graphene nucleation is significantly lower for atmospheric pressure CVD as compared to the low pressure CVD. It is moderately contributed by the partial sublimation of Cu under high temperature and low pressure, removing

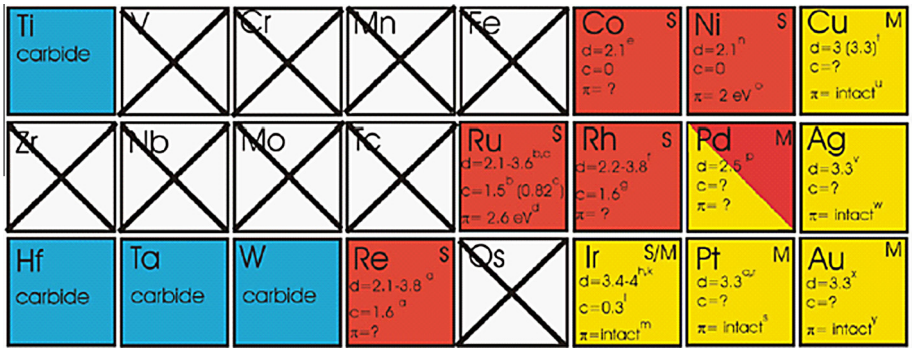


Fig. 2 – Summary of the interaction between graphene and transition metals. Yellow-labelled elements indicate weak interactions, and red and blue can be attributed to strong interactions and graphene grown from bulk carbide, respectively. "d" is the distance between graphene and metal (in scale of Angstrom), "c" indicates the buckling and corrugation of graphene (in scale of Angstrom), and "π" refers to the amount of downward shift of the Dirac point of graphene when mounted on respective transition metals [78]. (A color version of this figure can be viewed online.)

the carbon species adsorbed on the Cu surface and thus leading to lower nucleation density [76].

3. Catalysts

Fe, Ni, and Co are known to be active metal catalysts for the synthesis of CNTs through CVD. These transition metals have non-filled d-shells that enable them to adsorb and interact with the hydrocarbons that are used as the carbon sources [77]. Similarly, graphene synthesis requires the same transition metal group as CNT synthesis. Different metals each have their own unique mechanism for growing graphene. The quality of the graphene grown is dependent on the ability of the transition metal to facilitate hydrocarbon dehydrogenation and carbon segregation. The as-grown graphene would have different interaction strengths and growth mechanisms based on the substrate. Batzill [78] had summarised information on 11 different transition metals that possess different interaction properties with graphene. The information is shown in Fig. 2.

The study of the phase diagrams of the transition metals to carbon enables the researchers to predict the overall outcome of graphene synthesis. Fe, Co and Ni are the most common transition metals for the synthesis of CNTs. These metals are commonly having relatively high carbon solubility. From the phase diagram in Fig. 3, it is notable that the solubility of carbon can reach a maximum of 4.1 at.% and 2.7 at.% for Co and Ni, respectively. Fe is estimated to have the carbon solubility of >25 at.%. Ni and Co would form metastable carbide at high temperature and the maximum is at ~1600 K. For most of the CVD process, the temperature is operated at around 1000 °C. According to the phase diagrams, the solubility of carbon is ~0.6 at.% and ~0.9 at.% for Ni and Co, respectively. During the cooling stage, the carbon solubility decreases and the carbon precipitation gives the formation of graphene [79,80].

3.1. *Ru*

Ru, which has a hexagonal closest-packed (hcp) structure, is one of the foremost transition metals that is found to be capable of growing graphene, and the Ru(0001) surface is the most stable because of the hcp crystal structure. Ru has a carbon solubility of approximately 0.34 at.% at 1000 °C. Moreover, Ru always appears in single-crystalline form after heating, and this ensures a relative flatness and a lack of grain boundaries for growing uniform graphene [82]. These properties make Ru one of the most widely studied transition metals for graphene synthesis.

The growth of graphene is strongly related to the interaction between the metal and the graphene itself. Two types of interactions are identified, namely, physisorption and chemisorption. Graphene growth on Ru(0001) has been classified into the group of strong chemisorption interactions. The chemisorption occurs through hybridisation of the d-orbital of Ru and the C p_z orbital. The lattice mismatch between Ru(0001) surfaces and graphene is estimated to be 9.1%, which means 10 Ru lattice periodicities line up with 11 graphene periodicities [83,84], Ru(10 × 10) to graphene(11 × 11). However, this finding is controversial, as Ru(11 × 11) to graphene(12 × 12) [85] and Ru(25 × 25) to graphene(23 × 23) [86] have also been reported. This lattice mismatch caused the graphene to possess a corrugated surface when it was observed under a high-resolution electron microscope. As shown in Fig. 4, three different regions were formed, including ridges (bright spots), valleys (dark areas in the triangle), and medium heights (triangles). Fig. 4(a) and (c) provide a clearer picture of the stacking of graphene on the surface of Ru(0001). All the carbons in the carbon ring sit on top of the Ru atoms in the valley (dark areas), whereas a unit of carbon sits on top of one Ru atom in the medium-height zone. The ridge is sometimes called the top site, whereas the hcp site and the fcc site are called the intermediate region and the valley, respectively [87]. The interaction between graphene and the Ru surface is relatively weak at the ridge and relatively strong at the valley, resulting in a corrugated surface known as the Moiré pattern. However, the simulation run by Peng and Ahuja [88] found that metallic bonding exists between graphene and Ru, and so the graphene should be quasi-periodic and nearly flat when lying on a Ru(0001) surface.

In the hcp structure, (0001), which is the most thermodynamically stable facet [90], can be easily prepared at high tem-

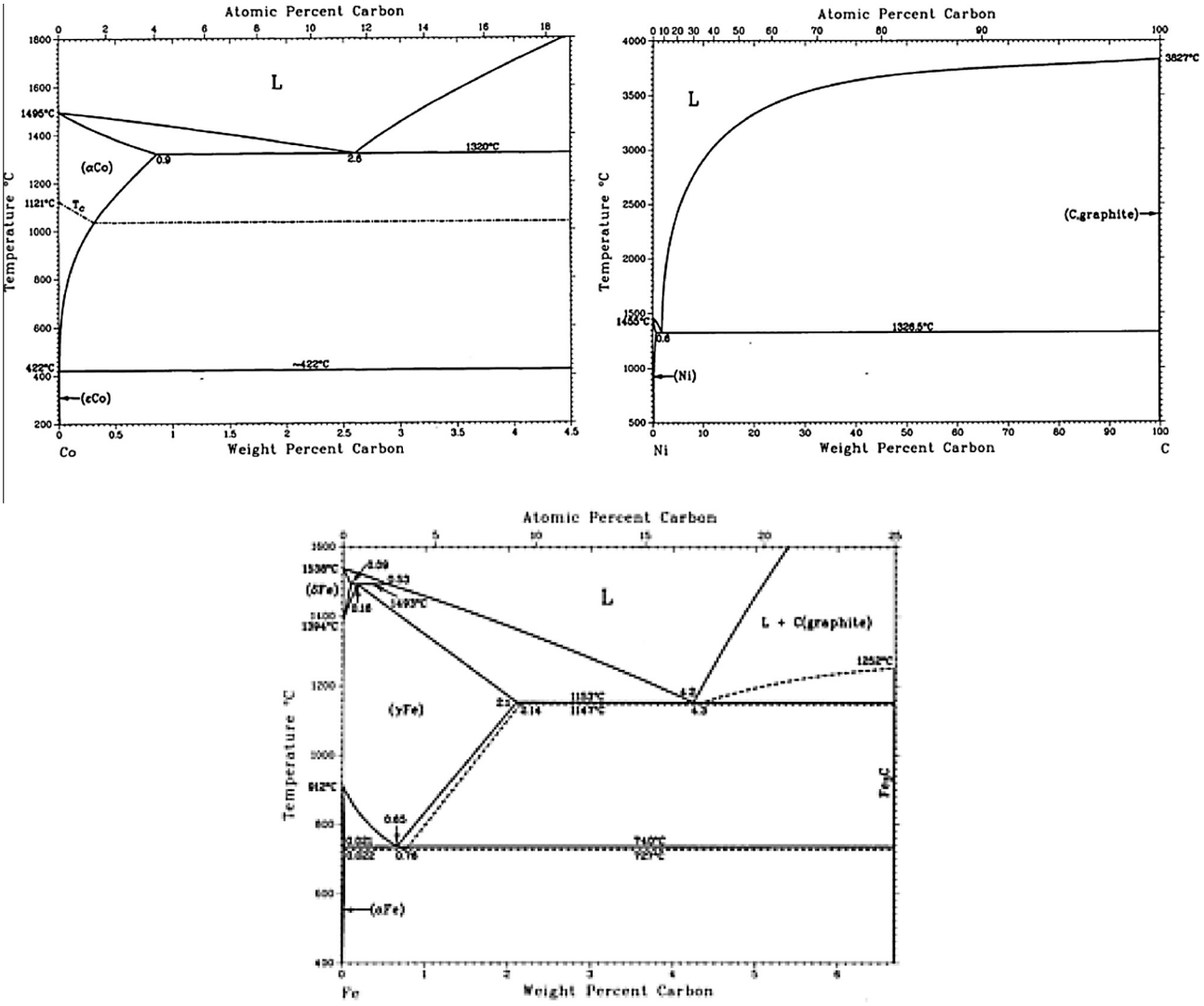


Fig. 3 – Binary phase diagram of Co–C, Fe–C and Ni–C [81].

peratures [91] or with the aid of remote plasma [92] to obtain a predominantly smooth single-crystalline surface. Normally, the graphene grows on Ru following the downhill carpet growth mode, in which the graphene nucleates at the atomic substrate step edge, forming a continuous graphene. The downhill growth mode is principally caused by the strong bonding between C and Ru [93]. This strong interaction yields an average interspacing of 0.145 nm between the graphene and the Ru surface, which is smaller than the step height of Ru, i.e., 0.220 nm [94]. According to Sutter et al., the hybridisation of the out-of-plane π-orbitals with the metal d-shell and the in-plane σ states participating in sp^2 bonding was distorted when the graphene edge met the elevated Ru step. The zigzag edge with localised dangling σ bonds was projected onto the atomic Ru uphill step, which maximised the orbital overlap and inhibited the growth uphill [94].

The well-recognised growth mechanism of graphene on a Ru(0001) surface involves the carpet growth mode, which is also shared by most of the transition metals for the growth of graphene. Through TPG, hydrocarbons are dissociated and adsorbed on the Ru surface, producing a layer of adsorbed hydrocarbon intermediates at room temperature. During the heating stage, the hydrocarbon intermediates will further dehydrogenate and decompose to form carbon clusters. The carbon clusters coalesce due to surface tension and form graphene after reaching saturation and during the cooling [55]. The McCarty research group has further studied the mechanism of graphene growth on the Ru(0001) surface. It was found that the nucleation of graphene started when the carbon adatoms dissolved in the Ru reached supersaturation [95]. The graphene growth rate was limited by the diffusion of carbon through the Ru bulk phase to the surface of the Ru [96]. McCarty and co-workers [95] presented an interesting finding on the growth mechanism. Initially, owing to the strong bond between Ru and carbon adatoms, the carbon that dissolved during the hydrocarbon dissociation most likely appears in the threefold hollow site between Ru atoms arranged in the hcp lattice, where the energy state is the lowest. The dissolved carbon must first break the strong bond with Ru to reach the nearest graphene edge located above the surface of Ru. The carbon must diffuse within the Ru lattice, shape the carbon cluster, and later lift the whole cluster

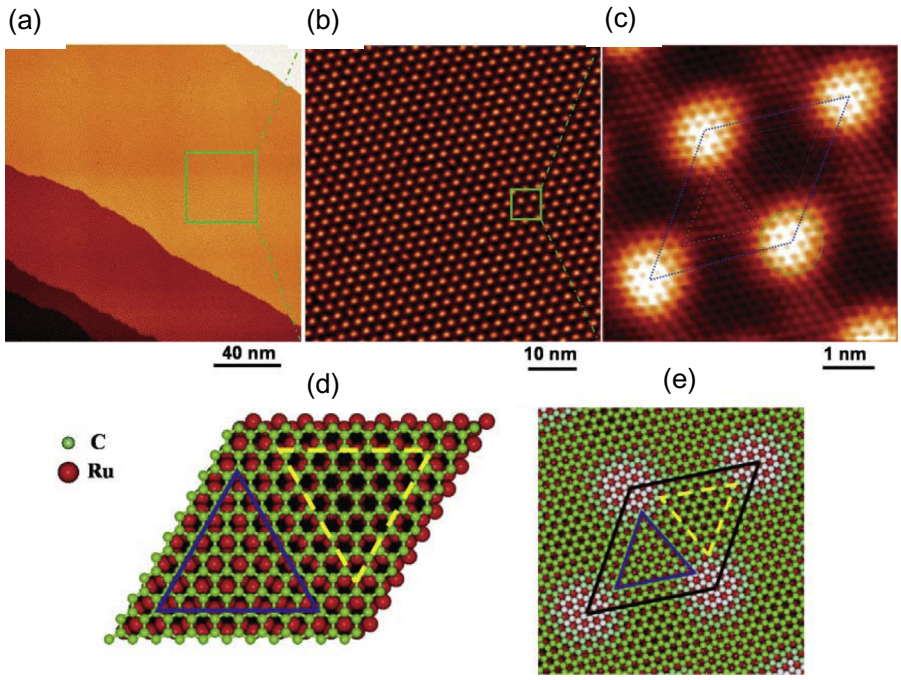


Fig. 4 – (a, b, and c) STM image for an atomic-resolution image of one unit cell of the Moiré pattern. (d) Illustration of the optimised atomic structure showing one unit cell of the superlattice. (e) An enlarged perspective view of the superlattice. [89]. (A color version of this figure can be viewed online.)

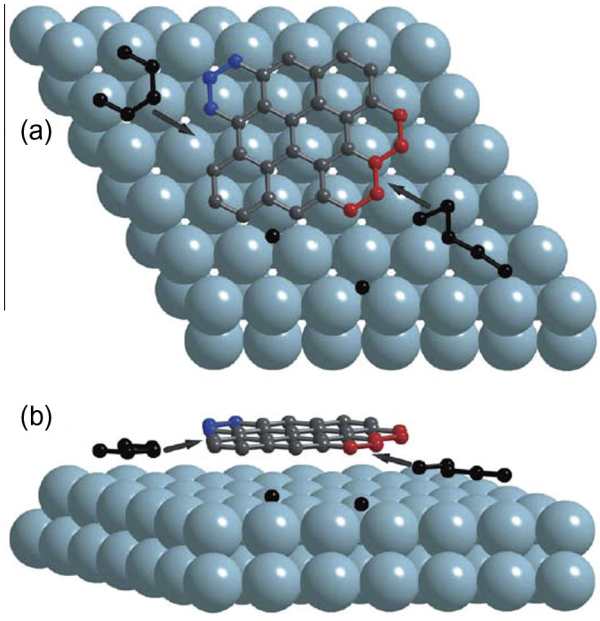


Fig. 5 – (a) top and (b) side views of graphene growth by attachment of C-atom clusters. Two 5-atom clusters (black) are sketched. Isolated C adatoms reside in the 3-fold hollow sites of the Ru substrate (green). At least three C atoms must be added to the *compact* graphene island (grey-shaded atoms) to form new six-membered rings. Adding three (blue) or five (red) C atoms makes one or two new six-membered rings, respectively [95]. (A color version of this figure can be viewed online.)

up and attach it to the graphene edge, as shown in Fig. 5. Furthermore, the cluster should have at least three (blue atoms in graphene in Fig. 5) or five (red) carbon atoms to be able to attach firmly onto the existing graphene edge, forming a new six-membered ring [97]. The same growth mechanism applies to other carbon sources used, but the rate of the carbon adatom generation and the graphene growth rate may vary depending on the source of carbon [18].

The interaction between graphene and Ru is strong, which causes alterations in the topography of the lattice steps on the Ru surface. The first layer of graphene is believed to be covalently bonded to the Ru atoms by the hybridisation of carbon $2p_z$ orbitals with Ru d-states near the Fermi level [94]. When the size of the graphene expands, the Ru atoms beneath the graphene are facing erosion during the advancement of the graphene front. Part of the Ru atoms on the upper terrace are removed by being shifted down by the graphene front as the seed for the graphene growth at the lower terrace [98]. Meanwhile, the line of the Ru step edge was also observed to change when graphene met the uphill step edge [93]. A majority of the Ru atoms were pushed to the upper terrace or intercalated beneath the graphene. Günther et al. [98] recorded different changes in the lattice step for different operating conditions. At a relatively high temperature and with a limited hydrocarbon feedstock, the graphene front no longer grows across the atomic step, either uphill or downhill, but flattens the surface of Ru. When the graphene front meets the edge of the lattice step, the Ru atoms from other areas are shifted to fill the growing step edge, where they underlay the graphene underlayer to smooth the Ru surface. This occurs due to the high temperature that provides energy for the diffusion of Ru atoms across

the step edges; meanwhile, a limited carbon source will slow down the growth of graphene and provide more time for Ru atoms to diffuse and flatten the surface. In addition, the strong graphene and Ru surface interaction cause the graphene flake that seeded on the Ru to have an asymmetrical shape. The hybridisation of the out-of-plane graphene π orbital with a metal d-band is too strong to disrupt the graphene growth when it reaches the step edge [99].

Jin et al. [100] employed a different Ru(0001) preparation to modify the graphene growth mode. The authors sputtered Ru in the presence of cycled Ar^+. The newly sputtered Ru trapped some Ar and formed bubbles, resulting in the surface of the Ru being full of protrusions. The protrusions stretched the Ru surface lattice and reduced the effect of the step edge. Thus, carbon clusters were able to attach to all edges of graphene, and this provoked growth in all directions rather than just downhill growth or growth along the step edge. According to Mavrikakis et al. [101], the stress on the surface of Ru(0001) caused a shift in the d-bands. The overlap between the d-electrons on the neighbouring metal atoms decreased due to the expanded lattice at the surface. The bandwidth decreased to keep the d-occupancy fixed, which subsequently increased the interaction of metal with the adsorbate. For multilayer graphene on Ru(0001), a bottom-up layer-by-layer growth mechanism was proposed [102]. The nucleation of the second layer began after the first monolayer of graphene islands expanded and connected to form a continuous sheet of monolayer graphene. The grown graphene would dissolve into the Ru at increased temperatures.

Ru is one of the best catalysts for the epitaxial growth of graphene. It is easy to obtain a single-crystal surface with an orientation of (0001), and the interstitial carbon solubility can be reduced by a factor of six upon cooling. Moreover, the segregation of carbon formed graphene with a monocrystalline domain with perfect rotation alignment, a low defect density, and thickness control [82,103]. Furthermore, the graphene grown from Ru is mostly free from wrinkles. The number of the graphene layers can be controlled by manipulating the growth temperature to limit the carbon solubility in Ru [102]. However, the downhill carpet growth mechanism of graphene on Ru that nucleates at the step edge would cause defects in the graphene when the islands meet, especially when islands from two different terraces are connected [95]. The strong interaction between the graphene and the Ru surface metal is likely to distort the high density of electron states around the Fermi level of graphene on the Ru surface, causing strong hybridisation of graphene and Ru states, which severely affects the electronic structure of graphene [104]. To date, there is no effective method to remove graphene that has been grown on Ru.

3.2. Ir

Ir(111) with an fcc crystal structure is capable of nucleating graphene. However, Ir has a low carbon solubility, and the interaction between the Ir surface and graphene is weaker than the interaction between the Ru surface and graphene. The most common graphene/Ir supercell is a graphene(10×10) adlayer on Ir(9×9) [105,106]. The lattice constant of graphene and the Ir(111) surface differ by approximately 10% at room temperature, causing a lattice mismatch and the same Moiré structure as seen with Ru(0001) [106]. However, the growth path of the graphene on Ir is slightly different compared with the growth on Ru. Graphene may grow in both the uphill and downhill directions across the lattice step. The main reason for Ir to overcome the lattice step is the large distance between the graphene plane and the Ir surface. The for hcp and fcc regions, respectively. Meanwhile, the largest distance between graphene and the Ir surface is 4.04 Å for a top-type region, whereas the step height is 2.2 Å [105]. This phenomena is attributed to the weak interaction between graphene and Ir [107]. The interactions between the two surfaces mainly involve physisorption with chemical modulation [108].

The nucleation mechanism of graphene on Ir(111) is quite similar to that of Ru(001). The growth of graphene follows the nonlinear kinetic model. The carbon has to first be dissolved into the Ir metal until it reaches supersaturation. According to the simulation reported by Wu et al. [109], compared with the terrace, the most stable site for carbon adatom adsorption is on the side of the step edge. It is unstable for carbon monomers to escape from the step edge to form graphene islands, and the dimers that would escape from the step edge are C_5, C_8, and C_{11} or larger, and these dimers would serve as the nucleus for further growth. The subsequent expansion of the graphene island requires a dimer of C_5, which is a relatively stable form [18]. The nucleation preferentially occurs at the step edge because of the rapid cluster growth at high temperatures and the occupation of the preferred configuration [110]. Coraux et al. [111] further explored the expansion of graphene islands, as shown in Fig. 6. The configuration with a $(10\bar{1})$ Ir step aligned along a $(11\bar{2}0)$ graphene step is the most energetically favourable configuration. During the growth, the Ir step reshapes itself to maximise the contact between Ir and graphene (Fig. 6b). The expansion of graphene will first take place at the lower terrace. The energy barrier to break the C–Ir bond needs to be overcome for ascending growth. The upper terrace growth has to take place across the substrate step along the Ir$(10\bar{1})$ direction (Fig. 6c). After the graphene has grown over the step, the reshaping of the Ir step will stop. Further growth of the graphene islands on the lower terrace requires that the islands match with a less favourable step orientation, which forms a tile boundary between islands that match differently oriented Ir substrate steps (Fig. 6d). Heptagon and pentagon carbon rings would be present to allow the domain to tilt.

The orientation of nucleated graphene may vary, even when above identical Ir surfaces. The dominant variant is the [1120] direction of graphene aligned along the [110] direction of Ir, which is called the R0 variant. Other than R0, other orientations such as R22 (graphene lattice rotated 22° from the R0 orientation), R26 [112], R14, R18.5, and R30 [113] have also been reported. Generally, the R0 orientation is first nucleated, and the other orientations form at the boundary of the R0 islands [109]. The actual reason for the formation of different orientations has yet to be verified. Loginova et al. [113] proposed two reasons for the formation of different orientations. First, it could be caused by the fact that the different orientations have different local energy minima per unit area. The graphene relax into and trap these energetic minima

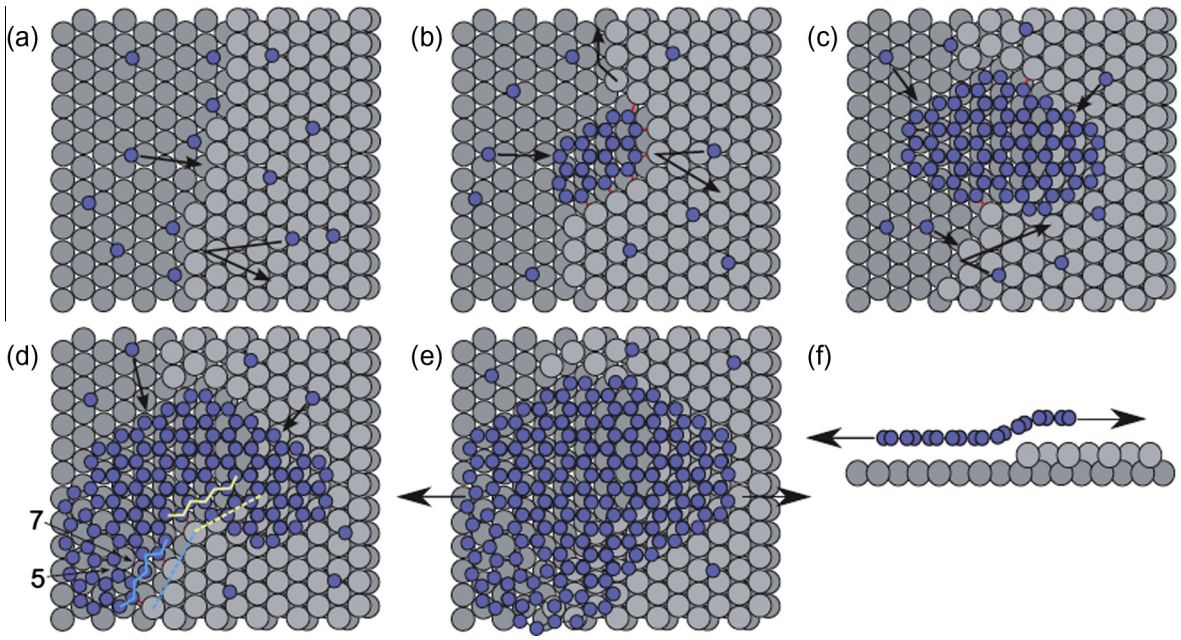


Fig. 6 – Top-view (a–e) and side-view (f) ball models of the growth of graphene on Ir(111). Carbon and iridium atoms are shown as purple and grey circles, respectively. Arrows schematically indicate either some of the atom movements (a–e) or the graphene growth rate (f). C–Ir bonds at the step edge are shown as red lines. Zigzag carbon edges of two misoriented domains are highlighted in (d) as thick solid lines; the undistorted zigzag edge lies parallel to the Ir(10$\bar{1}$) step edge highlighted as dotted lines (yellow). A heptagon–pentagon (7 and 5 labels in (d)) pair is present at the boundary between the two domains (d, e), allowing one domain to tilt. (A color version of this figure can be viewed online.)

after nucleation and later expand. The second explanation is more plausible: the different orientations could form during nucleation. This behaviour occurs because the graphene/Ir interaction is very small, which results in a very small elastic relaxation that causes orientation selection. However, the presence of different orientations indicates that the interaction between Ir and graphene is moderate, not strong enough to cause a uniform mismatch as with Ru, but strong enough to prevent free orientation. Different orientations were also observed in a single graphene island, where the growth rate was found to vary for different orientations of graphene flakes in which R0 was slower [18]. The nucleation of different orientations in a single graphene island was believed to be induced by the edge dislocation [114], and the graphene growth rate is caused by the difference in the binding energy of Ir to graphene of different orientations. The carbon attachment kinetics on graphene also varies for different orientations. For the nucleation of the second layer, it is more favourable for it to occur below the rotated variant than below the dominant domain. The rotated domain attaches to Ir metal weakly; thus, less energy is required for the de-bonding between the graphene and the Ir metal [112].

There are two methods used to increase the selectivity of the R0 variant of graphene on the Ir(111) surface. The first method is to increase the growth temperature. At a temperature of 1350 K, the majority of graphene is in a randomly rotated domain, whereas high selectivity of the R0 variant can be obtained at 1530 K [115]. Meanwhile, another proactive step involves using O_2 to etch away the rotated variants other than the R0 variant. The rotated domain is easier to etch away. The alternating exposure of precisely controlled hydrocarbon and O_2 would induce the cyclic growth of single-domain graphene, in which O_2 would etch away the rotated variant, leaving the exposed Ir surface for the graphene growth in the next cycle. The repeated cycles yield a single domain of graphene with high selectivity [116].

Ir is a unique transition metal that slightly distorts the electronic Dirac cone of pristine graphene [117]. As mentioned earlier, Ir has a low carbon solubility, which is useful for self-limiting the growth of graphene to a monolayer [114,118], although bilayer graphene is often obtained [112]. Graphene grown with Ir has major defects. Large-scale wrinkles are formed on the graphene during cooling. Some of the wrikle recorded are up to 0.55 nm from the adjacent surface. The main cause is the difference in the thermal contraction between Ir and graphene: Ir contracts 0.8% during cooling from 1000 °C to room temperature, whereas the thermal contraction of graphene is insignificant [113]. The effect that a multi-rotational variant would have on graphene grown on Ir remains unknown.

3.3. Pt

The use of Pt for hydrocarbon transformation can be traced back to the last few decades. Initially, the formation of carbon crystals on Pt was unwelcome due to the poisoning of the catalytic convertors in automobiles and the formation of coke in alkane transformation. Pt(111) has a weak interaction with graphene [52,119]. The reason for the weak interaction is similar to the case of Ir, which was mentioned in an earlier sec-

tion; the exposed outer electron 5d shell can only weakly interact with the π electron from graphene [120]. However, the interaction becomes stronger if a vacancy is introduced to the graphene [121]. The fact that binding between graphene and the Pt surface is weak allows graphene with random orientations to be present on the Pt surface [50], and 22 different Moiré superstructures have been reported [122]. Some researchers have categorised Pt into the same group as Cu in terms of the chemisorption/deposition growth mechanism due to the self-limiting growth mechanism and the epitaxial growth mechanism observed for bilayer graphene, which are similar to those seen in Cu [123,124].

Graphene can be fairly easily nucleated on Pt with various crystal facets, and the results vary under different operating conditions. The common Pt(111), Pt(110), Pt(100), and Pt(311) are able to grow graphene with ambient pressure CVD. Among these, Pt(111) is the most suitable for growing high-quality graphene, followed by Pt(110) and Pt(100) [125]. A large, continuous graphene has also been reported on Pt(100) [123]. Pt(311) only produces low-continuity graphene, which is attributed to the large lattice mismatch [125]. The work of Gao et al. showed that a millimetre-scale graphene could be formed even though a polycrystalline Pt surface was used [34]. Moreover, multi-crystalline graphene was reported to form on single-crystal Pt(111), and this occurred on the preferential decomposition of the grain boundaries with surface contamination.

Graphene shows both uphill and downhill directions of growth; the downhill growth is much faster, and the growth is carpet-mode growth, just like Ru and Ir [50]. Graphene has been observed to use step–mediated growth with surface restructuring, in which the graphene preferably nucleates from the step of the lattice [49]. Carbon atoms are mostly adsorbed at the fcc hollow sites of Pt films [126]. From the calculation by Viñes et al., adsorbed carbon atoms above 0.3 ML would induce aggregates of C_3 and C_2 species [126]. These carbon species will form graphene later. Meanwhile, the effect of graphene activity on the Pt surface remains uncertain. The observation of Fujita et al. showed that the graphene islands were hexagonal in shape and that they induced Pt atom rearrangement of the lower terrace [127]. Meanwhile, Land et al. reported a different finding in which irregular-shaped graphene islands were obtained and the upper lattice terrace was etched by the island during the graphene growth [128].

A large graphene grown on Pt also possesses wrinkles. The wrinkles can be attributed to the thermal contraction of Pt after cooling and the decrease in carbon density inside the metal after the depletion of the reservoir to form graphene [50]. However, the low solubility of carbon is the main reason Pt has a high selectivity towards monolayer graphene formation. The growth of a large-scale bilayer graphene film can be realised using a thicker Pt film with a single-crystal grain structure [51].

3.4. Ni

Ni is one of the most widely studied catalysts for the synthesis of graphene. The theory of nucleation on the Ni surface and the atomistic mechanism are still being debated. The high solubility of carbon enables single-crystalline Ni(111) and polycrystalline Ni to form graphene. The solubility of carbon in Ni was recorded as 0.9 at.% at 900 °C [16]. There is a significant hybridisation between the π orbitals and Ni d_{Z2}, which provides strong chemisorption between them, but at the same time, weak physisorption also exists at the hollow-site carbon p_z orbitals, where the hybridisation is lacking [129]. The lattice mismatch for Ni(111) is small, and no Moiré pattern can be observed [44]. However, there are other observations showing that a Moiré superstructure could be observed on both Ni(111) and Ni(110) [130,131]. The spacing between Ni atoms in the bulk phase is 2.49 Å, whereas the in-plane lattice parameter of graphite is 2.46 Å; the lattice mismatch is approximately 1% [132]. This would lead to epitactic growth with minimum additional strain induced in the graphene and would facilitate the growth of graphene on the Ni(111) surface [129].

The high performance of Ni has caused researchers to use Ni(111) as a substrate to study the atomistic mechanism involved in carbon adatoms forming graphene using different types of software. By using Density Functional Theory (DFT), it was proposed that the carbon adatoms are the first to form the chain cluster. It was found that the terminal atoms have a stronger interaction with the surface due to the local minima of the adsorption energy possessed by the chain cluster of carbons. Meanwhile, carbons in a single ring cluster cannot adhere to the Ni surface while maintaining their optimal gas-phase configurations and fulfil the constraints due to the epitaxial relationships [132]. Moreover, a single, small, six-member ring (MR) cluster is always found to not be stable on transition metal terraces [132–134]. The carbon chain cluster diffuses in the <110> direction of Ni(111). At the step edge, the ring cluster is more stable due to the enhanced activity of the metal step edge, and the aromatisation would occur there [134]. The transformation of the carbon chain into a hexagon ring would dissipate chemical potential energy, and this process is utilised for nucleation. The nucleation occurs mainly on the step edge, whereas nucleation at the terrace becomes significant at relatively high temperatures (>1272 K) and on a flat surface, which is caused by the lower barrier energy [134]. The finding is different when molecular dynamics (MD) or quantum chemical MD is carried out. The nucleation of graphene can be started with the aggregation of carbon on a plain transition metal surface under a high concentration of carbon. The initial nucleated graphitic structure is in a multi-MR, and the defect healing that occurs under high-temperature annealing increases the portion of six-MR carbon. Further healing and extension of the graphene island is completed by adding carbon adatoms rather than carbon clusters [135], as simulated by DFT. Wang et al. [136] claimed that Haeckelite structures are preferentially nucleated first and later healed by the Ni(111) surface to form graphene. During healing, the role of Ni is to provide rapid stabilisation for the system. The Ni atoms partially move out of the surface to stabilise the dangling σ-bonds during healing [136,137]. The Ni–C bonds keep breaking and reforming at the defect area for healing [138]. All the simulation results show that the pentagon and heptagon ring or Stone–Wales (SW)-like defects are rarely healed due to their energetic stability. The healing effect and mechanism have been verified in experimental work [137].

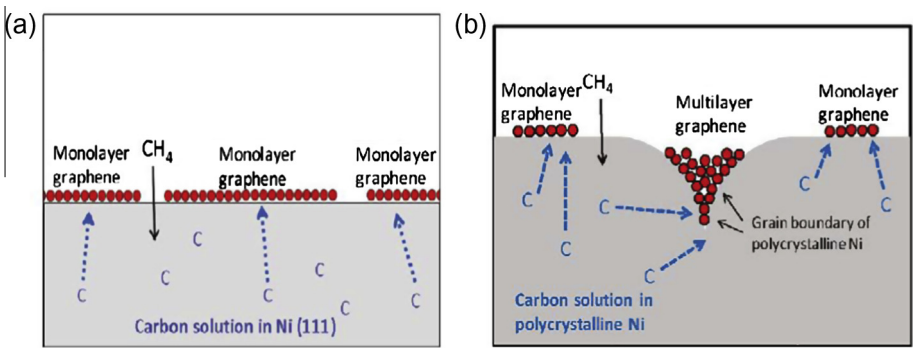


Fig. 7 – Graphene formation on (a) a single-crystal Ni(111) surface and (b) a polycrystalline Ni surface [139]. (A color version of this figure can be viewed online.)

Readily available polycrystalline Ni foil is also used to grow large-area graphene films. However, the graphene grown from the polycrystalline Ni is always found to have various thicknesses and numbers of layers [139–141] (Fig. 7). Polycrystalline Ni with a large number of grain boundaries contains a high density of lattice steps. Most of the multilayer graphene nucleates at these lattice steps [140]. This is because the curvature of the grain edge allows the accumulation of carbon at these sites for multilayer graphene nucleation, as shown in Fig. 7(b). Meanwhile, the smooth surface of single-crystal Ni(111) enhances the monolayer graphene nucleation [139] (Fig. 7(a)). The graphene formation temperature is different on different surfaces, and (001) is the lowest. The grown graphene was observed to dissolve back into Ni at 850 °C, whereas this is the ideal temperature for other surfaces to nucleate graphene [141]. Ni(001) has a strong binding energy with graphene because each carbon atom is in contact with four Ni atoms. The strong Ni–C interaction would cause a repulsive interaction within the C–C interaction and cause dissolution at the edge of graphene [141].

Multilayer graphene is always formed on polycrystalline Ni, which is attributable to its high solubility for carbon. Various methods are investigated to limit the graphene to monolayers and bilayers. These methods include controlling the carbon concentration in CVD and increasing the cooling rate after CVD. A high cooling rate will restrict excess carbon precipitation because there will be insufficient time for carbon atoms to diffuse [142]. However, when the carbon feedstock is low, a fast cooling rate causes little graphene coverage on the Ni surface [143]. The solubility of carbon in Ni can be reduced by lowering the growth temperature to approximately 550 °C to self-limit graphene segregation, but not too low as to form nickel carbide [144]. The surface of polycrystalline Ni can be polished by using a longer annealing time before CVD to induce the surface transformation that favours the formation of Ni(111) with fewer grain boundaries, thus inhibiting the multilayer graphene nucleation in the later CVD step [139]. The flatness of terraces can also be improved by using a better buffer layer, such as MgO deposited at low temperatures. A smooth Ni(111) surface can be formed by subsequent Ni deposition [145]. The high carbon solubility and high carbon diffusion rate in Ni can also be utilised to control the number of graphene layers formed. The dissolved carbon may diffuse through the Ni film, ultimately forming bilayer graphene in the middle of the Si substrate and the Ni film [70]. Xu et al. [46] directly deposited a Ni film on HOPG to synthesise monolayer graphene by carbon diffusion through a Ni film.

The graphene that grows on Ni is positioned uniquely in terms of the Ni configurations; fewer grain boundary defects can be observed on graphene when two islands coalesce due to the strong healing ability of Ni. The in-plane lattice constant for graphene expands by 1.2% from bulk graphite to match that of the Ni(111) substrate at room temperature. In contrast, Ni contracts 1% from 1100 K to room temperature, the thermal stress is reduced, and graphene that is free of wrinkles is obtained [43]. The as-grown graphene on Ni always consists of small individual graphene domains with different thicknesses, regardless of whether single-crystal or polycrystalline Ni is used, which is mainly caused by the large solubility of carbon in Ni [146]. Research involving Ni catalysts still remains in the preliminary stage, and precise control over graphene formation has yet to be achieved.

3.5. *Cu*

The discovery of Cu's ability to be used for graphene synthesis came later compared with other catalysts, as mentioned previously. As discussed in Section 2, the nucleation and extension mechanism of graphene catalysed by Cu is quite different; a chemisorption/deposition or surface growth approach has been proposed. The solubility of carbon in the Cu bulk is very low, and the mobility of carbon can be concluded to be a purely surface-based process [147]. In addition, the diffusion barrier of carbon atoms on Cu is also low [148], which gives Cu a different catalytic role compared with other transition metals. The Ruoff research group published several articles about alternating the exposure of $^{12}CH_4$ and $^{13}CH_4$ isotopes to copper foil [16,37,149]. The authors clearly showed that the growth front of graphene can be delineated by the boundaries between the domain of ^{12}C- and ^{13}C-based graphene (Fig. 8). The observations by Ruoff indicated that the growth of graphene on Cu was surface mediated and that limited diffusion of carbon into the Cu bulk occurred. Generally, the formation of graphene is initiated by nucleation at the initial instant of carbon precursor exposure, and the number of islands increases with exposure time to the carbon precursor.

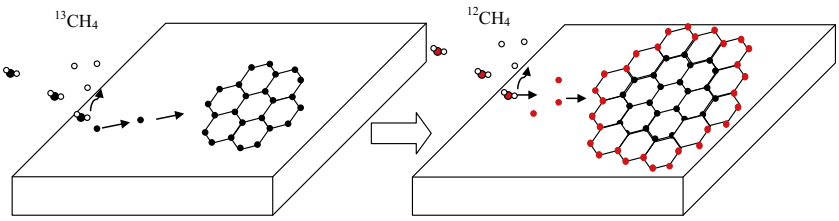


Fig. 8 – The surface growth mechanism. Black particles indicate ^{13}C isotope, particles indicate ^{12}C isotope and white particle indicates hydrogen [16]. (A color version of this figure can be viewed online.)

The carbon adatoms are found to interact mainly with free-electron–like surface states in Cu, leading to a weak surface diffusion barrier on the Cu surface [150]. The islands grow with time, whereas some of the islands may coalesce with other islands if the temperature is high [58,151]. The unique grow mechanism of graphene on Cu has enabled it to be self-limiting during graphene formation on Cu, thus yielding predominantly monolayer graphene with excellent quality [152].

The graphene islands tend to have an ordered shape, such as a hexagonal shape with 120° corners [41,99,147,153–155] (Fig. 9(a)), a flower-like shape with four or six lobes (Fig. 9(b)), or a dendrite shape (Fig. 9(c)). The hexagonal shape of graphene islands formed by the zigzag edge is preferred in graphene grown on polycrystalline Cu [153]. The low diffusion barrier of carbon on the Cu surface enables the carbon monomer to attach to the graphene islands on its own, which is different from the carbon cluster attachment on graphene for Ru and Ir. The DFT calculation by Luo et al. [99] shows that the carbon monomer attachment to the armchair edges is energetically favourable. The graphene grows by the mechanism of converting armchair edges to zigzag edges and maintains the growth of zigzag edges afterwards. In addition, the armchair-like edges are intended to be passivated by Cu atoms, and the passivation lowers the barrier for carbon atoms attaching to the graphene edge. This behaviour leads to the very fast growth of the armchair edge, and it gradually disappears, whereas the more inert zigzag edge grows slowly but dominates the growing graphene islands [147]. These mechanisms are only feasible under low-carbon-source conditions. In addition, the growth should occur at atmospheric pressure. The temperature must be high enough to support the molecular activity, or a dendritic domain will be obtained. If the growth duration is longer, the six corners of the hexagonal graphene islands will protrude to become six-petalled flower-like shapes [41].

The CVD of Cu under low-pressure conditions would also start with the nucleation of a large number of domains but with four-lobed flower-like [37,58,156,157] (Fig. 9(b)) or six-lobed flower-like [149,158] structures across the Cu surface. The understanding of the actual formation mechanism of those structures remains weak. There are several explanations proposed. First, the behaviour is attributed to the underlying Cu substrate: either the mobile carbon atoms on the surface or those carried by Cu atoms may diffuse along one of the four equivalent lattice axes of the substrate and extend the growth along one of the directions [157]. Wofford et al. believes the graphene islands undergo complex nucleation and simultaneously seed a graphene island with multiple orientations. The growth is faster at the four corners, which forms the four-lobed shape [156]. Full coverage of the Cu surface with monolayer graphene can be obtained through proper control of the operating parameters, such as the carbon precursor feed rate, temperature, pressure, and hydrogen ratio [37,158].

Graphene can be nucleated on various crystal facets on Cu, including Cu(310), Cu(410), Cu(411), Cu(433), Cu(632), Cu(100), and Cu(111) [159]. However, only Cu(100) and Cu(111) can outclass other facets. The graphene formed on Cu(001) is polycrystalline [157]. The carbon diffusion is slower on Cu(100) and may cause carbon stacking to form multilayer graphene [159]. However, a continuous graphene can be obtained through proper manipulation of the process parameters [160]. Tao et al. pre-annealed a Cu(111) film to form a continuous graphene with the help of a co-catalyst, hydrogen [161]. The performance of Cu(111) is better than that of

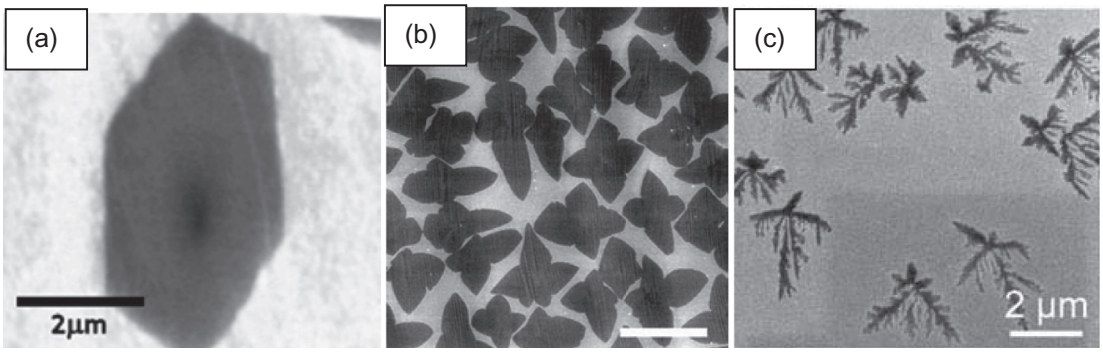


Fig. 9 – SEM images for graphene with (a) a hexagonal shape [154], (b) a four-lobed flower shape [37], and (c) a dendrite shape [41].

Cu(001) in the formation of monolayer graphene with a single domain [159,160,162]. The higher binding energy of graphene on Cu(111) ensures the graphene is in the most energetically stable state on Cu(111) to prevent other orientations and grain defects [163]. The presence of different graphene orientations on Cu(100) would cause defects at the graphene grain boundaries when graphene islands meet and grow [164]. Zhao et al. also found that the graphene on Cu(111) has a hexagonal superstructure, whereas the superstructure is linear on Cu(100) and it is not uniform [164]. In contrast, four different graphene variations can be found on a single graphene island nucleated at the same site on Cu(100) due to surface imperfections that induce complex heterogeneous nucleation events [156]. Meanwhile, the triangular (111) crystal has a greater similarity with the hexagonal graphene lattice in terms of crystallographic geometry and a lower energy barrier for nucleation that results from a smaller lattice mismatch [165]. Wu et al. [166] made a different observation, in which graphene formed equally on Cu surfaces with any crystal lattice, but Cu(111) formed rectangle graphene islands instead of the hexagonal graphene islands that are normally found. The small and different graphene orientation on Cu(111) was also found by Gao et al. [167]. The formation of a different graphene orientation on Cu(111) is generated by misalignment during the growth across the step edge. However, the problem of multiple orientations can be reduced by using higher growth temperatures and smoother Cu surfaces either in high-vacuum or atmospheric-pressure CVD [74,168]. As reported by Walter et al. [169], the multiple orientation of domains can be found on both Cu(111) and Cu(100) surfaces when relatively low temperatures (850–900 °C) are used for graphene growth.

Polycrystalline Cu foil is the preferred catalyst because it is easy to obtain at low cost compared with single-crystal Cu surfaces. In addition, the Cu substrate would end up with scarification from graphene separation. Furthermore, the single-crystal Cu requires a longer exposure to harsh chemicals to fully etch it away, which will damage the graphene [170]. Various observations have been reported on graphene grown from polycrystalline Cu substrates. Both single-crystal graphene [155,171] and polycrystalline graphene [74,156,172] have been reported to form on polycrystalline Cu. The polycrystalline Cu contains the largest number of atomic steps and grain boundaries, and these sites always have a higher chemical activation energy for hydrocarbon decomposition and serve as the sites for graphene nucleation [37,156,172]. It has also been reported that the nucleation of graphene is a random event [36]. Although low-pressure CVD and similar operating conditions were used, many articles reported that the grain size of Cu has no effect on the grain size of the graphene formed [23,58]. Wood et al. [159] reported that graphene can be nucleated on any crystal facet of polycrystalline Cu, but only the Cu(111) surface promotes fast monolayer graphene growth with fewer defects. The graphene grown from Cu(111) will spill over to other facets and may cover the existing graphene island on the other facets, thus forming graphene with non-uniform layers. Under prolonged growth with the assistance of plasma, the graphene would be lifted up to form graphene nanowalls [27]. The defects at the grain boundary have also been reported to serve as a channel for the diffusion of carbon adatoms to the non-exposed bottom surface of Cu, thus forming graphene at both surfaces [73].

Although it has always been believed that Cu possesses the ability to form predominantly monolayer graphene, some researchers have started to question this ability of Cu, especially under atmospheric-pressure CVD, as discussed in previous section. Bhaviripudi et al. [32] found that monolayer graphene could only be grown under atmospheric pressure with methane on the ppm scale, and the general crystallinity of graphene is also poor due to the low mass transport rate of the carbon source. The formation of multilayer graphene is induced by the high level of precursor saturation due to excess supply [154]. It is believed that the projected density of states (PDOS) of the underlying Cu may penetrate through the graphene. The PDOS would dissociate the carbon precursor above the graphene and cause the formation of subsequent layers of graphene [173]. Moreover, the boundaries of graphene grains and the impurities that lie on graphene can provide nucleation sites for additional layer of graphene [75], and it is believed that the subsequent layer of graphene grows on top of the first layer of graphene [174]. Zhang et al. [175] demonstrated a different view in which a C–Cu alloy exists during the whole graphene formation process. The authors proposed a new mechanism in which the carbon atoms that adsorb on the Cu surface first form a C–Cu alloy. This alloy provides the carbon source for the graphene extension. The carbon rich C–Cu alloy will provide the carbon source for the subsequent layer.

The study of the synthesis of graphene on Cu has flourished since the first report by Li et al. [152] in 2009. However, the understanding of the kinetics and the mechanisms of graphene formation is still lacking. There are many mysteries yet to discover and many theories waiting to be verified. Cu has been proven to outperform other metals, such as Ru, Ir, and Pt, in terms of cost-effective graphene growth. However, there are also drawbacks to the use of Cu, such as the appearance of wrinkles on the graphene and structural defects at the joints of graphene islands due to different crystallinities. Pentagon or heptagon carbon rings do always appear which will limit the application of graphene in the field of electronics.

3.6. *Others*

Co(0001) has a structure quite similar to that of Ni(111), as both have in-plane lattice constants that match that of graphene; the lattice mismatch is less than 2% [65]. Co has a high carbon solubility but a low carbon diffusion coefficient [176]. Fast cooling is required after CVD to enhance the graphene formation; otherwise, the carbon atoms will diffuse deeper into the Co film, which causes no graphene to be formed. The oxide of Co, i.e., Co_3O_4(111), was also found to form graphene [177]. The graphene on Co_3O_4 was found to possess a dielectric response similar to that of graphene on SiO_2 or SiC, which can directly be applied in CMOS technology. In addition to Co and Ni, iron in the form of a thin film [178] and conventional iron foil [79] have been used in graphene synthesis. However, the result is not satisfactory, as the high carbon solubility in iron leads to the formation of iron carbide

[179–182] and limits the formation of monolayer graphene. In addition, graphene with a large number of defects is normally observed on iron. In contrast, the graphene formed on Rh is highly corrugated due to the strong chemisorption and the lattice mismatch [120]. However, theoretically, the bonding between graphene and Rh should not be strong, based on its position in the periodic table [183]. This can be explained by Rh preferring the bridge arrangement, in which the incomplete charge transfers in antibonding states of carbon-π orbitals to destabilise the interaction to weaken the binding [184]. High-quality graphene can be formed on Rh, but no detailed mechanism has been reported thus far [185]. Pd(111) was reported to grow graphene following the carpeting growth mechanism, similar to Ru (0001) [186]. Six different orientations of graphene in a single sample were observed by Murata et al. [187], but single-domain graphene has also been successfully grown [188]. Other metal catalysts, such as gold [189], were found to possess the ability to perform graphene nucleation, but knowledge of these catalysts is limited, and more studies are required to further identify the feasibility of these metal catalysts.

The transition metals as mentioned above possessing its own advantages and shortcomings, respectively. In order to combine the stronghold of each respective transition metal, bi- or more metallic catalysts are been designed and used for the graphene synthesis research.

The combination of Ni–Cu is the most common and most broadly reported; Cu and Ni have a very distinct solubility of carbon under various recipe of Cu–Ni, which allows the management of carbon solubility for optimisation of growth of graphene. There are 2 type of common Ni–Cu combination. First is the direct using of Ni–Cu alloy or by coating the bimetallic film in nanocale. The nanoscale metals will partially molten under high temperature annealing. Both Ni and Cu atoms will diffuse into each other due high miscibility between both metals. The control of graphene to monolayer becomes much easier by manipulating the lower growth temperature, faster cooling rate and less composition of Ni [190–192]. Meanwhile, if the temperature is not high enough, presence of Ni carbide would break up the Ni with surrounding metal, forming nanoparticle, subsequently induced the nucleation of CNTs [193]. But for full coverage, it still required higher temperature and slower cooling rate. The purely surface mediated growth mechanism is broken with addition of Ni, even with 5.5% of Ni, replaced with bottom-up supply mode of carbon source [191,194]. A small amount of Ni can be used to enhance the self-limiting ability of Cu to precisely control the graphene layer formation [190]. However, an alloy with a large amount of Ni is no different than pure Ni. Besides that, the different lattice structure shows a very distinct variation on the energy barrier on the dehydrogenation. Cu/Ni(111) shows a much higher dehydrogenation energy barrier, while Cu/Ni(100) is about 40–60% lower compared with Cu/Ni(111) [195]. Another type is the separated bilayer Ni–Cu alloy. It composes a composite substrate with C-dissolving (Ni) layer and a C-rejecting (Cu) layer, where the Cu mainly to inhibit the diluted carbon [196].

Ni and Cu with high activity to graphene formation are also been alloyed with other transition metals to improve the quality of graphene. Mo that coated with thin film of Ni

Table 1 – General properties of transition metals.

Transition metals	Growth mechanism	Carbon solubility at ~1000 °C	Active crystal cacet	Spacing between graphene to transition metals	Max size of grown graphene up to date (in market or in research)
Ru	Bulk-mediated growth, carpet growth mode	0.34 at.% [82]	Ru(0001)	1.45–2.20 Å [94]	In research scale
Ir	Bulk-mediated growth, carpet growth mode	0.041 at.% [82]	Ir(111)	3.77–4.04 Å [105]	In research scale
Pt	Still in debate either bulk-mediated growth or surface-mediated growth	~3.1×10^{-4}–0.0043 at.% [124,202,203]	Pt(111) (the best performance), Pt(110), Pt(100), Pt(311),	3.23–3.67 Å [204]	In research scale
Ni	Bulk-mediated growth	~0.6–0.9 at.% [16,81]	All facets are active. Ni(111) with the best performance	2.46–2.49 Å [132]	2″ × 4″ by graphene supermarket
Cu	Surface-mediated growth	~7.4×10^{-4}–0.008 at.% [32,80,81,205]	All facets are active, Cu(100) and Cu(111) with the best performance	3.26–3.708 Å [206,207]	24″ × 300″ by bluestone global tech

thin film had been verified to produce ultimately monolayer graphene and full surface coverage, under wide variations of operating conditions [197]. The alloying of gold on surface would boost the reactivity of catalyst and high coverage of graphene can be obtained under 450 °C [198]. Meanwhile monolayer graphene also can be obtained by alloying small amount of Ni onto gold surface, but with higher temperature [29]. The purpose of gold is to suppress the dissolute carbon into Ni. Tri-metallic alloys, Fe–Ni–Cr also been reported, but the outcome is not optimist [199]. A very thick layer of Cu that melted on Mo giving a highly oriented graphene but lack of coverage [200]. The graphene that grown on Cu not fully alloyed with other metal was similar with pure Cu.

Alloy that free from Cu or Ni is rare, but a unique polycrystalline $Pt_{83}Rh_{17}$ was used for graphene formation [201]. However, the graphene is not uniform. The implication of alloy into the graphene synthesis is a new branch of research. To date, it is still in the initial stage. The role each element in the alloy is yet to be well understood, neither the most common alloy, Ni–Cu. The line of the synthesis of graphene is still wide, broad variety of alloys with different elements and composition yet to be studied. Table 1 summarise general properties of transition metals.

4. Future prospects

Knowledge about graphene synthesis by CVD is still incomplete, and the controllable growth of graphene is still unachievable. There is also no direct observation on how the metal crystal structure affects the segregation of carbon from the metal to form the graphene. The role of the transition metal in changing the chemical state of the graphene edge during the fusing of two graphene islands has yet to be discovered. Another issue is that the majority of the growth conditions for CVD involve Ultra-High Vacuum (UHV) and high temperatures, which would increase the production cost. A single-crystal transition metal substrate is difficult to obtain, and synthesising single-crystal graphene from transition metals is rather difficult; the problem becomes more complicated if a large-area single-crystal metal substrate is required [140]. Roll-to-roll methods have been applied for the continuous synthesis of large-area graphene [26,208], which may be a platform for mass production. However, the huge amount of metal foil consumption and as-grown graphene with many defects remain the key obstacles for mass production. After many years of research, ambient-pressure CVD and polycrystalline metal have been proven to be workable in growing graphene. Although plasma-enhanced CVD or cold-wall CVD was reported to reduce the growth temperature for graphene formation, lower-quality graphene was the compensation.

The use of expensive metals such as Ru, Ir, Pt, and Pd for the synthesis of graphene is not practical. Moreover, those metals are relatively inert, which makes the separation of graphene from the catalyst substrate difficult. The separation approach normally involves etching the substrate. However, this process will consume the substrate and cause severe defects in the graphene. Reuse of the catalyst substrate is the most crucial step to reducing the production cost and facilitating large-area graphene production. It has been reported [34,209] that graphene can be separated from Pt and Cu substrates by bubbling transfer using electrochemical delamination. In this process, water is reduced electrochemically, and the hydrogen bubbles that are formed detach the graphene from the substrate. The damage that would be caused to the single-crystal metal surface remains unknown, and the process is slow. In contrast, the direct peel-off method using thermal release tape for graphene separation always causes mechanical damage to the graphene. An easy method to weaken the interaction strength between graphene and the substrate is needed to enable the direct peel-off of graphene without deteriorating the surface of substrate, especially for a single-crystalline surface. There is a report that using liquid form catalyst, Ga and other Sn and In alloys to form graphene. The catalyst is removed by using syringe. It simplify the separation process [210], but there still a lot of technical problem to be solve, like how to control the unstable liquid surface and etc.

Another challenge is to grow large-area single-crystal graphene. The most ideal graphene is a flat single crystal with no defects, which will be uniformly reactive. However, graphene tends to nucleate at random sites on the metal substrate with various orientations. Moreover, the orientation may change as the graphene grows over the lattice steps. Once the graphene has become large, shifting the orientation is impossible. Some researchers have proposed inhibiting the nucleation site of the graphene island. However, this method would require a very smooth metal surface with minimum step edges, and this would slow down the graphene growth rate. A more innovative approach is required.

5. Summary

Graphene is an innovative material that possesses various desirable properties, and CVD appears to be the most promising route for accomplishing large-area graphene synthesis in a scalable way. Among all the metals that have been studied for graphene formation, Ni and Cu are the two transition metals with the potential for synthesising large-area graphene with ease. Studies are required to achieve controllable synthesis, which includes the ability to tailor and fabricate the size and the number of layer of graphene. This can only be achieved if the graphene growth mechanism, kinetics, and rate-limiting step are revealed and new classes of catalysts and processing conditions are discovered. Effective separation and reuse of the catalysts would be the key obstacle for the mass production of graphene at low cost. The rapid pace of graphene research ensures that a more practical graphene synthesis and transfer method will be discovered. There are many challenges and opportunities for applications in daily life.

Acknowledgements

The authors gratefully acknowledge the financial support provided by Universiti Sains Malaysia (USM Fellowship), the

AEX-Delivery Excellence grant (APEX-DE 2012), and E-Science Fund (Dana Pembiayaan Program Konsortia Penyelidikan Graphene).

REFERENCES

[1] Bianco A, Cheng H-M, Enoki T, Gogotsi Y, Hurt RH, Koratkar N, et al. All in the graphene family: a recommended nomenclature for two-dimensional carbon materials. Carbon 2013;65:1–6.

[2] Novoselov KS, Geim AK, Morozov SV, Jiang D, Zhang Y, Dubonos SV, et al. Electric field effect in atomically thin carbon films. Science 2004;306(5696):666–9.

[3] Mermin ND, Wagner H. Absence of ferromagnetism or antiferromagnetism in one- or two-dimensional isotropic Heisenberg models. Phys Rev Lett 1966;17(22):1133–6.

[4] Mermin ND. Crystalline order in two dimensions. Phys Rev 1968;176(1):250–4.

[5] Ijima S. Helical microtubules of graphitic carbon. Nature 1991;354(6348):56–8.

[6] Liang YT, Hersam MC. Highly concentrated graphene solutions via polymer enhanced solvent exfoliation and iterative solvent exchange. J Am Chem Soc 2010;132(50):17661–3.

[7] Zhu Y, Murali S, Cai W, Li X, Suk JW, Potts JR, et al. Graphene and graphene oxide: synthesis, properties, and applications. Adv Mater 2010;22(35):3906–24.

[8] Hummers WS, Offeman RE. Preparation of graphitic oxide. J Am Chem Soc 1958;80(6):1339.

[9] Staudenmaier L. Verfahren zur Darstellung der Graphitsäure. Berichte der deutschen chemischen Gesellschaft 1898;31(2):1481–7.

[10] Allen MJ, Tung VC, Kaner RB. Honeycomb carbon: a review of graphene. Chem Rev 2009;110(1):132–45.

[11] Pei S, Cheng H-M. The reduction of graphene oxide. Carbon 2012;50(9):3210–28.

[12] McAllister MJ, Li J-L, Adamson DH, Schniepp HC, Abdala AA, Liu J, et al. Single sheet functionalized graphene by oxidation and thermal expansion of graphite. Chem Mater 2007;19(18):4396–404.

[13] Lee JH, Shin DW, Makotchenko VG, Nazarov AS, Fedorov VE, Kim YH, et al. One-step exfoliation synthesis of easily soluble graphite and transparent conducting graphene sheets. Adv Mater 2009;21(43):4383–7.

[14] Robinson J, Weng X, Trumbull K, Cavalero R, Wetherington M, Frantz E, et al. Nucleation of epitaxial graphene on SiC(0001). ACS Nano 2009;4(1):153–8.

[15] Shelton JC, Patil HR, Blakely JM. Equilibrium segregation of carbon to a nickel (111) surface: a surface phase transition. Surf Sci 1974;43(2):493–520.

[16] Li X, Cai W, Colombo L, Ruoff RS. Evolution of graphene growth on Ni and Cu by carbon isotope labeling. Nano Lett 2009;9(12):4268–72.

[17] Eizenberg M, Blakely JM. Carbon monolayer phase condensation on Ni(111). Surf Sci 1979;82(1):228–36.

[18] Loginova E, Bartelt NC, Feibelmarr PJ, McCarty KF. Factors influencing graphene growth on metal surfaces. New J Phys 2009;11.

[19] Losurdo M, Giangregorio MM, Capezzuto P, Bruno G. Graphene CVD growth on copper and nickel: role of hydrogen in kinetics and structure. Phys Chem Chem Phys 2011;13(46):20836–43.

[20] Kralj M, Pletikosić I, Petrović M, Pervan P, Milun M, N'Diaye AT, et al. Graphene on Ir(111) characterized by angle-resolved photoemission. Phys Rev B - Condens Matter Mater Phys 2011;84(7).

[21] Kalita G, Wakita K, Umeno M. Low temperature growth of graphene film by microwave assisted surface wave plasma CVD for transparent electrode application. RSC Adv 2012;2(7):2815–20.

[22] Qi JL, Zheng WT, Zheng XH, Wang X, Tian HW. Relatively low temperature synthesis of graphene by radio frequency plasma enhanced chemical vapor deposition. Appl Surf Sci 2011;257(15):6531–4.

[23] Terasawa T-o, Saiki K. Growth of graphene on Cu by plasma enhanced chemical vapor deposition. Carbon 2012;50(3):869–74.

[24] Levchenko I, Volotskova O, Shashurin A, Raitses Y, Ostrikov K, Keidar M. The large-scale production of graphene flakes using magnetically-enhanced arc discharge between carbon electrodes. Carbon 2010;48(15):4570–4.

[25] Volotskova O, Levchenko I, Shashurin A, Raitses Y, Ostrikov K, Keidar M. Single-step synthesis and magnetic separation of graphene and carbon nanotubes in arc discharge plasmas. Nanoscale 2010;2(10):2281–5.

[26] Yamada T, Ishihara M, Kim J, Hasegawa M, Iijima S. A roll-to-roll microwave plasma chemical vapor deposition process for the production of 294 mm width graphene films at low temperature. Carbon 2012;50(7):2615–9.

[27] Kumar A, Voevodin AA, Zemlyanov D, Zakharov DN, Fisher TS. Rapid synthesis of few-layer graphene over Cu foil. Carbon 2012;50(4):1546–53.

[28] Nang LV, Kim ET. Controllable synthesis of high-quality graphene using inductively-coupled plasma chemical vapor deposition. J Electrochem Soc 2012;159(4). K93-K6.

[29] Woo YS, Seo DH, Yeon D-H, Heo J, Chung H-J, Benayad A, et al. Low temperature growth of complete monolayer graphene films on Ni-doped copper and gold catalysts by a self-limiting surface reaction. Carbon 2013;64:315–23.

[30] Gao L, Ren W, Zhao J, Ma L-P, Chen Z, Cheng H-M. Efficient growth of high-quality graphene films on Cu foils by ambient pressure chemical vapor deposition. Appl Phys Lett 2010;97(18). 183109-3.

[31] Zhang Y, Li Z, Kim P, Zhang L, Zhou C. Anisotropic hydrogen etching of chemical vapor deposited graphene. ACS Nano 2012;6(1):126–32.

[32] Bhaviripudi S, Jia X, Dresselhaus MS, Kong J. Role of kinetic factors in chemical vapor deposition synthesis of uniform large area graphene using copper catalyst. Nano Lett 2010;10(10):4128–33.

[33] Vlassiouk I, Regmi M, Fulvio P, Dai S, Datskos P, Eres G, et al. Role of hydrogen in chemical vapor deposition growth of large single-crystal graphene. ACS Nano 2011;5(7):6069–76.

[34] Gao L, Ren W, Xu H, Jin L, Wang Z, Ma T, et al. Repeated growth and bubbling transfer of graphene with millimetre-size single-crystal grains using platinum. Nat Commun 2012;3:699.

[35] Memon NK, Tse SD, Chhowalla M, Kear BH. Role of substrate, temperature, and hydrogen on the flame synthesis of graphene films. Proc Combust Inst 2013;34(2):2163–70.

[36] Regmi M, Chisholm MF, Eres G. The effect of growth parameters on the intrinsic properties of large-area single layer graphene grown by chemical vapor deposition on Cu. Carbon 2012;50(1):134–41.

[37] Li X, Magnuson CW, Venugopal A, An J, Suk JW, Han B, et al. Graphene films with large domain size by a two-step chemical vapor deposition process. Nano Lett 2010;10(11):4328–34.

[38] Vlassiouk I, Smirnov S, Ivanov I, Fulvio PF, Dai S, Meyer H, et al. Electrical and thermal conductivity of low

temperature CVD graphene: the effect of disorder. Nanotechnology 2011;22(27).
[39] Li Z, Wu P, Wang C, Fan X, Zhang W, Zhai X, et al. Low-temperature growth of graphene by chemical vapor deposition using solid and liquid carbon sources. ACS Nano 2011;5(4):3385–90.
[40] Rasool HI, Song EB, Allen MJ, Wassei JK, Kaner RB, Wang KL, et al. Continuity of graphene on polycrystalline copper. Nano Lett 2011;11(1):251–6.
[41] Fan L, Li Z, Li X, Wang K, Zhong M, Wei J, et al. Controllable growth of shaped graphene domains by atmospheric pressure chemical vapour deposition. Nanoscale 2011;3(12):4946–50.
[42] Liu N, Fu L, Dai B, Yan K, Liu X, Zhao R, et al. Universal segregation growth approach to wafer-size graphene from non-noble metals. Nano Lett 2011;11(1):297–303.
[43] Odahara G, Otani S, Oshima C, Suzuki M, Yasue T, Koshikawa T. Macroscopic single-domain graphene sheet on Ni(111). Surf Interface Anal 2011;43(12):1491–3.
[44] Lahiri J, Miller T, Adamska L, Oleynik II, Batzill M. Graphene growth on Ni(111) by transformation of a surface carbide. Nano Lett 2011;11(2):518–22.
[45] Lahiri J, Miller TS, Ross AJ, Adamska L, Oleynik II, Batzill M. Graphene growth and stability at nickel surfaces. New J Phys 2011;13.
[46] Xu M, Fujita D, Sagisaka K, Watanabe E, Hanagata N. Production of extended single-layer graphene. ACS Nano 2011;5(2):1522–8.
[47] Jacobson P, Stöger B, Garhofer A, Parkinson GS, Schmid M, Caudillo R, et al. Nickel carbide as a source of grain rotation in epitaxial graphene. ACS Nano 2012;6(4):3564–72.
[48] Grüneis A, Kummer K, Vyalikh DV. Dynamics of graphene growth on a metal surface: a time-dependent photoemission study. New J Phys 2009;11.
[49] Peng Z, Somodi F, Helveg S, Kisielowski C, Specht P, Bell AT. High-resolution in situ and ex situ TEM studies on graphene formation and growth on Pt nanoparticles. J Catal 2012;286:22–9.
[50] Sutter P, Sadowski JT, Sutter E. Graphene on Pt(111): growth and substrate interaction. Phys Rev B 2009;80(24):245411.
[51] Yong V, Hahn HT. Graphene growth with giant domains using chemical vapor deposition. CrystEngComm 2011;13(23):6933–6.
[52] Gao M, Pan Y, Huang L, Hu H, Zhang LZ, Guo HM, et al. Epitaxial growth and structural property of graphene on Pt(111). Appl Phys Lett 2011;98(3):033101–33103.
[53] Sutter P, Hybertsen MS, Sadowski JT, Sutter E. Electronic structure of few-layer epitaxial graphene on Ru(0001). Nano Lett 2009;9(7):2654–60.
[54] Yi P, Shi D, Gao HJ. Formation of graphene on Ru(0001) surface. Chin Phys B 2007;16(11):3151–3.
[55] Zhang H, Fu Q, Cui Y, Tan D, Bao X. Growth mechanism of graphene on Ru(0001) and O_2 adsorption on the graphene/Ru(0001) surface. J Phys Chem C 2009;113(19):8296–301.
[56] Nandamuri G, Roumimov S, Solanki R. Chemical vapor deposition of graphene films. Nanotechnology 2011;21(14):145604.
[57] Yao Y, Li Z, Lin Z, Moon K-S, Agar J, Wong C. Controlled growth of multilayer, few-layer, and single-layer graphene on metal substrates. J Phys Chem C 2011;115(13):5232–8.
[58] Hwang C, Yoo K, Kim SJ, Seo EK, Yu H, Biró LP. Initial stage of graphene growth on a Cu substrate. J Phys Chem C 2011;115(45):22369–74.
[59] Guermoune A, Chari T, Popescu F, Sabri SS, Guillemette J, Skulason HS, et al. Chemical vapor deposition synthesis of graphene on copper with methanol, ethanol, and propanol precursors. Carbon 2011;49(13):4204–10.
[60] Kishi N, Fukaya A, Sugita R, Kado T, Soga T, Jimbo T. Synthesis of graphenes on Ni foils by chemical vapor deposition of alcohol with IR-lamp heating. Mater Lett 2012;79:21–4.
[61] Choi J-H, Li Z, Cui P, Fan X, Zhang H, Zeng C, et al. Drastic reduction in the growth temperature of graphene on copper via enhanced London dispersion force. Sci Rep 2013;3:1925.
[62] Xue Y, Wu B, Jiang L, Guo Y, Huang L, Chen J, et al. Low temperature growth of highly nitrogen-doped single crystal graphene arrays by chemical vapor deposition. J Am Chem Soc 2012;134(27):11060–3.
[63] Gan X, Zhou H, Zhu B, Yu X, Jia Y, Sun B, et al. A simple method to synthesize graphene at 633K by dechlorination of hexachlorobenzene on Cu foils. Carbon 2012;50(1):306–10.
[64] Cai J, Ruffieux P, Jaafar R, Bieri M, Braun T, Blankenburg S, et al. Atomically precise bottom-up fabrication of graphene nanoribbons. Nature 2012;466(7305):470–3.
[65] Eom D, Prezzi D, Rim KT, Zhou H, Lefenfeld M, Xiao S, et al. Structure and electronic properties of graphene nanoislands on Co(0001). Nano Lett 2009;9(8):2844–8.
[66] Cui Y, Fu Q, Zhang H, Bao X. Formation of identical-size graphene nanoclusters on Ru(0001). Chem Commun 2011;47(5):1470–2.
[67] Seo JH, Lee HW, Kim J-K, Kim D-G, Kang J-W, Kang M-S, et al. Few layer graphene synthesized by filtered vacuum arc system using solid carbon source. Curr Appl Phys 2012;12(Suppl. 2(0)). S131-S3.
[68] Ji H, Hao Y, Ren Y, Charlton M, Lee WH, Wu Q, et al. Graphene growth using a solid carbon feedstock and hydrogen. ACS Nano 2011;5(9):7656–61.
[69] Sun Z, Yan Z, Yao J, Beitler E, Zhu Y, Tour JM. Growth of graphene from solid carbon sources. Nature 2010;468(7323):549–52.
[70] Peng Z, Yan Z, Sun Z, Tour JM. Direct growth of bilayer graphene on SiO_2 substrates by carbon diffusion through nickel. ACS Nano 2012;5(10):8241–7.
[71] Ruan G, Sun Z, Peng Z, Tour JM. Growth of graphene from food, insects, and waste. ACS Nano 2011;5(9):7601–7.
[72] Ray AK, Sahu RK, Rajinikanth V, Bapari H, Ghosh M, Paul P. Preparation and characterization of graphene and Ni-decorated graphene using flower petals as the precursor material. Carbon 2012;50(11):4123–9.
[73] Su C-Y, Lu A-Y, Wu C-Y, Li Y-T, Liu K-K, Zhang W, et al. Direct formation of wafer scale graphene thin layers on insulating substrates by chemical vapor deposition. Nano Lett 2011;11(9):3612–6.
[74] Nie S, Wofford JM, Bartelt NC, Dubon OD, McCarty KF. Origin of the mosaicity in graphene grown on Cu(111). Phys Rev B 2011;84(15):155425.
[75] Yan K, Peng H, Zhou Y, Li H, Liu Z. Formation of bilayer bernal graphene: layer-by-layer epitaxy via chemical vapor deposition. Nano Lett 2011;11(3):1106–10.
[76] Vlassiouk I, Smirnov S, Regmi M, Surwade SP, Srivastava N, Feenstra R, et al. Graphene nucleation density on copper: fundamental role of background pressure. J Phys Chem C 2013;117(37):18919–26.
[77] Seah C-M, Chai S-P, Mohamed AR. Synthesis of aligned carbon nanotubes. Carbon 2011;49(14):4613–35.
[78] Batzill M. The surface science of graphene: metal interfaces, CVD synthesis, nanoribbons, chemical modifications, and defects. Surf Sci Rep 2012;67(3–4):83–115.
[79] An H, Lee WJ, Jung J. Graphene synthesis on Fe foil using thermal CVD. Curr Appl Phys 2011;11(Suppl. 4). S81-S5.
[80] Mattevi C, Kim H, Chhowalla M. A review of chemical vapour deposition of graphene on copper. J Mater Chem 2011;21(10):3324–34.
[81] ASM Hanbook, ASM International. Alloy Phase Diagrams 2002.

[82] Arnoult WJ, McLellan RB. The solubility of carbon in rhodium ruthenium, iridium and rhenium. Scr Metallurgica 1972;6(10):1013–8.
[83] Jia-Tao S, Shi-Xuan D, Wen-De X, Hao H, Yu-Yang Z, Guo L, et al. Effect of strain on geometric and electronic structures of graphene on a Ru(0001) surface. Chin Phys B 2009;18(7):3008–13.
[84] VÃzquez de Parga AL, Calleja F, Borca B, Passeggi Jr MCG, Hinarejos JJ, Guinea F, et al. Periodically rippled graphene: growth and spatially resolved electronic structure. Phys Rev Lett 2008;100(5):056807.
[85] Marchini S, Günther S, Wintterlin J. Scanning tunneling microscopy of graphene on Ru(0001). Phys Rev B 2007;76(7):075429.
[86] Martoccia D, Willmott PR, Brugger T, Björk M, Günther S, Schlepütz CM, et al. Graphene on Ru(0001): a 25Ã—25 supercell. Phys Rev Lett 2008;101(12):126102.
[87] Feng W, Lei S, Li Q, Zhao A. Periodically modulated electronic properties of the epitaxial monolayer graphene on Ru(0001). J Phys Chem C 2011;115(50):24858–64.
[88] Peng X, Ahuja R. Epitaxial graphene monolayer and bilayers on Ru(0001): Ab initio calculations. Phys Rev B 2010;82(4):045425.
[89] Pan Y, Zhang H, Shi D, Sun J, Du S, Liu F, et al. Highly ordered, millimeter-scale, continuous, single-crystalline graphene monolayer formed on Ru (0001). Adv Mater 2009;21(27):2777–80.
[90] Kim H, Koseki T, Ohba T, Ohta T, Kojima Y, Sato H, et al. Effect of Ru crystal orientation on the adhesion characteristics of Cu for ultra-large scale integration interconnects. Appl Surf Sci 2006;252(11):3938–42.
[91] Lee H-Y, Hsieh Y-W, Hsu CH, Liang KS. Characteristics of sputter-deposited Ru thin films on Si substrates. Mater Chem Phys 2003;82(3):984–90.
[92] Kwon O-K, Kwon S-H, Park H-S, Kang S-W. Plasma-enhanced atomic layer deposition of ruthenium thin films. Electrochem Solid-State Lett 2004;7(4). C46-C8.
[93] Starodub E, Maier S, Stass I, Bartelt NC, Feibelman PJ, Salmeron M, et al. Graphene growth by metal etching on Ru(0001). Phys Rev B 2009;80(23):235422.
[94] Sutter PW, Flege JI, Sutter EA. Epitaxial graphene on ruthenium. Nat Mater 2008;7(5):406–11.
[95] Loginova E, Bartelt NC, Feibelman PJ, McCarty KF. Evidence for graphene growth by C cluster attachment. New J Phys 2008;10.
[96] McCarty KF, Feibelman PJ, Loginova E, Bartelt NC. Kinetics and thermodynamics of carbon segregation and graphene growth on Ru(0001). Carbon 2009;47(7):1806–13.
[97] Zangwill A, Vvedensky DD. Novel growth mechanism of epitaxial graphene on metals. Nano Lett 2011;11(5):2092–5.
[98] GuÎnther S, GuÎnther S, Wang B, Bocquet ML, Schmitt S, Wintterlin J. Single Terrace growth of graphene on a metal surface. Nano Lett 2011;11(5):1895–900.
[99] Luo Z, Kim S, Kawamoto N, Rappe AM, Johnson ATC. Growth mechanism of hexagonal-shape graphene flakes with zigzag edges. ACS Nano 2011;5(11):9154–60.
[100] Jin L, Fu Q, Zhang H, Mu R, Zhang Y, Tan D, et al. Tailoring the growth of graphene on Ru(0001) via engineering of the substrate surface. J Phys Chem C 2012;116(4):2988–93.
[101] Mavrikakis M, Hammer B, Nørskov JK. Effect of strain on the reactivity of metal surfaces. Phys RevLett 1998;81(13):2819–22.
[102] Cui Y, Fu Q, Bao X. Dynamic observation of layer-by-layer growth and removal of graphene on Ru(0001). Phys Chem Chem Phys 2010;12(19):5053–7.
[103] Sutter E, Albrecht P, Sutter P. Graphene growth on polycrystalline Ru thin films. Appl Phys Lett 2009;95(13).
[104] Brugger T, Günther S, Wang B, Dil JH, Bocquet M-L, Osterwalder J, et al. Comparison of electronic structure and template function of single-layer graphene and a hexagonal boron nitride nanomesh on Ru(0001). Phys Rev B 2009;79(4):045407.
[105] N'Diaye AT, Bleikamp S, Feibelman PJ, Michely T. Two-dimensional Ir cluster lattice on a graphene Moiré on Ir(111). Phys Rev Lett 2006;97(21):215501.
[106] Brako R, Šokčević D, Lazić P, Atodiresei N. Graphene on the Ir(111) surface: from van der Waals to strong bonding. New J Phys 2010;12.
[107] Gong C, Lee G, Shan B, Vogel EM, Wallace RM, Cho K. First-principles study of metal–graphene interfaces. J Appl Phys 2010;108(12):123711–8.
[108] Busse C, Lazić P, Djemour R, Coraux J, Gerber T, Atodiresei N, et al. Graphene on Ir(111): physisorption with chemical modulation. Phys Rev Lett 2011;107(3):036101.
[109] Wu P, Jiang H, Zhang W, Li Z, Hou Z, Yang J. Lattice mismatch induced nonlinear growth of graphene. J Am Chem Soc 2012;134(13):6045–51.
[110] Lacovig P, Pozzo M, Alfè D, Vilmercati P, Baraldi A, Lizzit S. Growth of dome-shaped carbon nanoislands on Ir(111): the intermediate between carbidic clusters and quasi-free-standing graphene. Phys Rev Lett 2009;103(16):166101.
[111] Coraux J, N'Diaye AT, Engler M, Busse C, Wall D, Buckanie N, et al. Growth of graphene on Ir(111). New J Phys 2009;11:023006.
[112] Nie S, Walter AL, Bartelt NC, Starodub E, Bostwick A, Rotenberg E, et al. Growth from below: graphene bilayers on Ir(111). ACS Nano 2011;5(3):2298–306.
[113] Loginova E, Nie S, Thürmer K, Bartelt NC, McCarty KF. Defects of graphene on Ir(111): rotational domains and ridges. Phys Rev B 2009;80(8):085430.
[114] Coraux J, N'Diaye AT, Busse C, Michely T. Structural coherency of graphene on Ir(111). Nano Lett 2008;8(2):565–70.
[115] Hattab H, N'Diaye AT, Wall D, Jnawali G, Coraux J, Busse C, et al. Growth temperature dependent graphene alignment on Ir(111). Appl Phy Lett 2011;98(14). 141903-3.
[116] van Gastel R, N'Diaye AT, Wall D, Coraux J, Busse C, Buckanie NM, et al. Selecting a single orientation for millimeter sized graphene sheets. Appl Phys Lett 2009;95(12):121901–3.
[117] Pletikosić I, Kralj M, Pervan P, Brako R, Coraux J, N'Diaye AT, et al. Dirac cones and minigaps for graphene on Ir(111). Phys Rev Lett 2009;102(5):056808.
[118] N'Diaye AT, Coraux J, Plasa TN, Busse C, Michely T. Structure of epitaxial graphene on Ir(111). New J Phys 2008;10.
[119] Politano A, Marino AR, Chiarello G. Phonon dispersion of quasi-freestanding graphene on Pt(111). J Phys: Condens Matter 2012;24(10):104025.
[120] Preobrajenski AB, Ng ML, Vinogradov AS, Mårtensson N. Controlling graphene corrugation on lattice-mismatched substrates. Phys Rev B 2008;78(7):073401.
[121] Ugeda MM, Fernández-Torre D, Brihuega I, Pou P, Martínez-Galera AJ, Pérez R, et al. Point defects on graphene on metals. Phys Rev Lett 2011;107(11):116803.
[122] Merino P, Švec M, Pinardi AL, Otero G, Martín-Gago JA. Strain-driven moiré superstructures of epitaxial graphene on transition metal surfaces. ACS Nano 2011;5(7):5627–34.
[123] Nilsson L, Andersen M, Bjerre J, Balog R, Hammer B, Hornekær L, et al. Preservation of the Pt(100) surface reconstruction after growth of a continuous layer of graphene. Surf Sci 2012;606(3–4):464–9.
[124] Kang BJ, Mun JH, Hwang CY, Cho BJ. Monolayer graphene growth on sputtered thin film platinum. J Appl Phys 2009;106(10). 104309-6.

[125] Gao T, Xie S, Gao Y, Liu M, Chen Y, Zhang Y, et al. Growth and atomic-scale characterizations of graphene on multifaceted textured pt foils prepared by chemical vapor deposition. ACS Nano 2011;5(11):9194–201.
[126] Viñes F, Neyman KM, Görling A. Carbon on platinum substrates: from carbidic to graphitic phases on the (111) surface and on nanoparticles. J Phys Chem A 2009;113(43):11963–73.
[127] Fujita T, Kobayashi W, Oshima C. Novel structures of carbon layers on a Pt(111) surface. Surf Interface Anal 2005;37(2):120–3.
[128] Land TA, Michely T, Behm RJ, Hemminger JC, Comsa G. STM investigation of single layer graphite structures produced on Pt(111) by hydrocarbon decomposition. Surf Sci 1992;264(3):261–70.
[129] Mittendorfer F, Garhofer A, Redinger J, Klimeš J, Harl J, Kresse G. Graphene on Ni(111): strong interaction and weak adsorption. Phys Rev B 2011;84(20):201401.
[130] Murata Y, Petrova V, Kappes BB, Ebnonnasir A, Petrov I, Xie Y-H, et al. Moiré superstructures of graphene on faceted nickel islands. ACS Nano 2010;4(11):6509–14.
[131] Fedorov AV, Varykhalov AY, Dobrotvorskii AM, Chikina AG, Adamchuk VK, Usachov DY. Structure of graphene on the Ni(110) surface. Phys Solid State 2011;53(9):1952–6.
[132] Cheng D, Barcaro G, Charlier J-C, Hou M, Fortunelli A. Homogeneous nucleation of graphitic nanostructures from carbon chains on Ni(111). J Phys Chem C 2011;115(21):10537–43.
[133] Gao J, Yuan Q, Hu H, Zhao J, Ding F. Formation of carbon clusters in the initial stage of chemical vapor deposition graphene growth on Ni(111) surface. J Phys Chem C 2011;115(36):17695–703.
[134] Gao J, Yip J, Zhao J, Yakobson BI, Ding F. Graphene nucleation on transition metal surface: structure transformation and role of the metal step edge. J Am Chem Soc 2011;133(13):5009–15.
[135] Meng L, Sun Q, Wang J, Ding F. Molecular dynamics simulation of chemical vapor deposition graphene growth on Ni (111) surface. J Phys Chem C 2012;116(10):6097–102.
[136] Wang Y, Page AJ, Nishimoto Y, Qian H-J, Morokuma K, Irle S. Template effect in the competition between haeckelite and graphene growth on Ni(111): quantum chemical molecular dynamics simulations. J Am Chem Soc 2011;133(46):18837–42.
[137] Jacobson P, Stöger B, Garhofer A, Parkinson GS, Schmid M, Caudillo R, et al. Disorder and defect healing in graphene on Ni(111). J Phys Chem Lett 2012;3(1):136–9.
[138] Karoui S, Amara H, Bichara C, Ducastelle F. Nickel-Assisted healing of defective graphene. ACS Nano 2010;4(10): 6114–20.
[139] Zhang Y, Gomez L, Ishikawa FN, Madaria A, Ryu K, Wang C, et al. Comparison of graphene growth on single-crystalline and polycrystalline Ni by chemical vapor deposition. The J Phys Chem Lett 2010;1(20):3101–7.
[140] Reina A, Jia X, Ho J, Nezich D, Son H, Bulovic V, et al. Large Area, few-layer graphene films on arbitrary substrates by chemical vapor deposition. Nano Lett 2008;9(1):30–5.
[141] Takahashi K, Yamada K, Kato H, Hibino H, Homma Y. In situ scanning electron microscopy of graphene growth on polycrystalline Ni substrate. Surf Sci 2012;606(7–8):728–32.
[142] Odahara G, Hibino H, Nakayama N, Shimbata T, Oshima C, Otani S, et al. Macroscopic single-domain graphene growth on polycrystalline nickel surface. Appl Phys Exp 2012;5(3).
[143] Reina A, Thiele S, Jia X, Bhaviripudi S, Dresselhaus MS, Schaefer JA, et al. Growth of large-area single- and bi-layer graphene by controlled carbon precipitation on polycrystalline Ni surfaces. Nano Res 2009;2(6):509–16.
[144] Addou R, Dahal A, Sutter P, Batzill M. Monolayer graphene growth on Ni(111) by low temperature chemical vapor deposition. Appl Phys Lett 2012;100(2):021601–21603.
[145] Iwasaki T, Park HJ, Konuma M, Lee DS, Smet JH, Starke U. Long-range ordered single-crystal graphene on high-quality heteroepitaxial Ni thin films grown on MgO(111). Nano Lett 2011;11(1):79–84.
[146] Sutter PW, Albrecht PM, Sutter EA. Graphene growth on epitaxial Ru thin films on sapphire. Appl Phys Lett 2010;97(21).
[147] Shu H, Chen X, Tao X, Ding F. Edge structural stability and kinetics of graphene chemical vapor deposition growth. ACS Nano 2012;6(4):3243–50.
[148] Yazyev OV, Pasquarello A. Effect of metal elements in catalytic growth of carbon nanotubes. Phys Rev Lett 2008;100(15):156102.
[149] Li X, Magnuson CW, Venugopal A, Tromp RM, Hannon JB, Vogel EM, et al. Large-area graphene single crystals grown by low-pressure chemical vapor deposition of methane on copper. J Am Chem Soc 2011;133(9):2816–9.
[150] Chen H, Zhu W, Zhang Z. Contrasting behavior of carbon nucleation in the initial stages of graphene epitaxial growth on stepped metal surfaces. Phys Rev Lett 2010;104(18):186101.
[151] Kim H, Mattevi C, Calvo MR, Oberg JC, Artiglia L, Agnoli S, et al. Activation energy paths for graphene nucleation and growth on Cu. ACS Nano 2012;6(4):3614–23.
[152] Li X, Cai W, An J, Kim S, Nah J, Yang D, et al. Large-area synthesis of high-quality and uniform graphene films on copper foils. Science 2009;324(5932):1312–4.
[153] Yu Q, Jauregui LA, Wu W, Colby R, Tian J, Su Z, et al. Control and characterization of individual grains and grain boundaries in graphene grown by chemical vapour deposition. Nat Mater 2011;10(6):443–9.
[154] Robertson AW, Warner JH. Hexagonal single crystal domains of few-layer graphene on copper foils. Nano Lett 2011;11(3):1182–9.
[155] Wu W, Jauregui LA, Su Z, Liu Z, Bao J, Chen YP, et al. Growth of single crystal graphene arrays by locally controlling nucleation on polycrystalline Cu using chemical vapor deposition. Adv Mater 2011;23(42):4898–903.
[156] Wofford JM, Nie S, McCarty KF, Bartelt NC, Dubon OD. Graphene islands on Cu foils: the interplay between shape, orientation, and defects. Nano Lett 2010;10(12): 4890–6.
[157] Rasool HI, Song EB, Mecklenburg M, Regan BC, Wang KL, Weiller BH, et al. Atomic-scale characterization of graphene grown on copper (100) single crystals. J Am Chem Soc 2011;133(32):12536–43.
[158] Zhang Y, Zhang L, Kim P, Ge M, Li Z, Zhou C. Vapor trapping growth of single-crystalline graphene flowers: synthesis, morphology, and electronic properties. Nano Lett 2012;12(6):2810–6.
[159] Wood JD, Schmucker SW, Lyons AS, Pop E, Lyding JW. Effects of polycrystalline Cu substrate on graphene growth by chemical vapor deposition. Nano Lett 2011;11(11):4547–54.
[160] Ogawa Y, Hu B, Orofeo CM, Tsuji M, Ikeda K-i, Mizuno S, et al. Domain structure and boundary in single-layer graphene grown on Cu(111) and Cu(100) films. J Phys Chem Lett 2012;3(2):219–26.
[161] Tao L, Lee J, Chou H, Holt M, Ruoff RS, Akinwande D. Synthesis of high quality monolayer graphene at reduced temperature on hydrogen-enriched evaporated copper (111) films. ACS Nano 2012;6(3):2319–25.
[162] Ishihara M, Koga Y, Kim J, Tsugawa K, Hasegawa M. Direct evidence of advantage of Cu(111) for graphene synthesis by using Raman mapping and electron backscatter diffraction. Mater Lett 2011;65(19–20):2864–7.

[163] Shi X, Yin Q, Wei Y. A theoretical analysis of the surface dependent binding, peeling and folding of graphene on single crystal copper. Carbon 2012;50(8):3055–63.
[164] Zhao L, Rim KT, Zhou H, He R, Heinz TF, Pinczuk A, et al. Influence of copper crystal surface on the CVD growth of large area monolayer graphene. Solid State Commun 2011;151(7):509–13.
[165] Hu B, Ago H, Orofeo CM, Ogawa Y, Tsuji M. On the nucleation of graphene by chemical vapor deposition. New J Chem 2012;36(1):73–7.
[166] Wu YA, Robertson AW, Schäffel F, Speller SC, Warner JH. Aligned rectangular few-layer graphene domains on copper surfaces. Chem Mater 2011;23(20):4543–7.
[167] Gao L, Guest JR, Guisinger NP. Epitaxial graphene on cu(111). Nano Lett 2010;10(9):3512–6.
[168] Hu B, Ago H, Ito Y, Kawahara K, Tsuji M, Magome E, et al. Epitaxial growth of large-area single-layer graphene over Cu(111)/sapphire by atmospheric pressure CVD. Carbon 2012;50(1):57–65.
[169] Walter AL, Nie S, Bostwick A, Kim KS, Moreschini L, Chang YJ, et al. Electronic structure of graphene on single-crystal copper substrates. Phys Rev B 2011;84(19):195443.
[170] Reddy KM, Gledhill AD, Chen C-H, Drexler JM, Padture NP. High quality, transferrable graphene grown on single crystal Cu(111) thin films on basal-plane sapphire. Appl Phys Lett 2011;98(11). 113117-3.
[171] Radhakrishnan G, Adams PM, Stapleton AD, Muller HG, Foran BJ. Large single-crystal monolayer graphene by decomposition of methanol. Appl Phys A: Mater Sci Process 2011;105(1):31–7.
[172] Liu W, Li H, Xu C, Khatami Y, Banerjee K. Synthesis of high-quality monolayer and bilayer graphene on copper using chemical vapor deposition. Carbon 2011;49(13):4122–30.
[173] Jeon I, Yang H, Lee S-H, Heo J, Seo DH, Shin J, et al. Passivation of metal surface states: microscopic origin for uniform monolayer graphene by low temperature chemical vapor deposition. ACS Nano 2011;5(3):1915–20.
[174] Kalbac M, Frank O, Kavan L. The control of graphene double-layer formation in copper-catalyzed chemical vapor deposition. Carbon 2012;50(10):3682–7.
[175] Zhang J, Hu P, Wang X, Wang Z. Structural evolution and growth mechanism of graphene domains on copper foil by ambient pressure chemical vapor deposition. Chem Phys Lett 2012;536:123–8.
[176] Koh ATT, Foong YM, Chua DHC. Comparison of the mechanism of low defect few-layer graphene fabricated on different metals by pulsed laser deposition. Diamond Relat Mater 2012;25:98–102.
[177] Mi Z, Frank LP, Peter AD, Alex B, Mathias S, Vanya D, et al. Direct graphene growth on Co_3O_4 (111) by molecular beam epitaxy. J Phys: Condens Matter 2012;24(7): 072201.
[178] Kondo D, Sato S, Yagi K, Harada N, Sato M, Nihei M, et al. Low-temperature synthesis of graphene and fabrication of top-gated field effect transistors without using transfer processes. Appl Phys Exp 2010;3(2).
[179] Seah C-M, Chai S-P, Ichikawa S, Mohamed AR. Synthesis of single-walled carbon nanotubes over a spin-coated Fe catalyst in an ethanol-PEG colloidal solution. Carbon 2012;50:960–7.
[180] Seah CM, Chai SP, Ichikawa S, Mohamed AR. Growth of uniform thin-walled carbon nanotubes with spin-coated Fe catalyst and the correlation between the pre-growth catalyst size and the nanotube diameter. J Nanopart Res 2013;15(1):1–10.
[181] Seah CM, Chai SP, Ichikawa S, Mohamed AR. Parametric study of methane catalytic CVD into single-walled carbon nanotubes using spin-coated iron nanoparticles. Chem Vap Deposition 2013;19(1–3):53–60.
[182] Seah CM, Chai SP, Ichikawa S, Mohamed AR. Control of iron nanoparticle size by manipulating PEG-ethanol colloidal solutions and spin-coating parameters for the growth of single-walled carbon nanotubes. Particuology 2013;11(4):394–400.
[183] Wang B, Caffio M, Bromley C, Früchtl H, Schaub R. Coupling epitaxy, chemical bonding, and work function at the local scale in transition metal-supported graphene. ACS Nano 2010;4(10):5773–82.
[184] Iannuzzi M, Hutter J. Comparative study of the nature of chemical bonding of corrugated graphene on Ru(0001) and Rh(111) by electronic structure calculations. Surf Sci 2011;605(15–16):1360–8.
[185] Roth S, Osterwalder J, Greber T. Synthesis of epitaxial graphene on rhodium from 3-pentanone. Surf Sci 2011;605(9–10). L17-L9.
[186] Kwon S-Y, Ciobanu CV, Petrova V, Shenoy VB, Bareo J, Gambin V, et al. Growth of semiconducting graphene on palladium. Nano Lett 2009;9(12):3985–90.
[187] Murata Y, Starodub E, Kappes BB, Ciobanu CV, Bartelt NC, McCarty KF, et al. Orientation-dependent work function of graphene on Pd(111). Appl Phys Lett 2010;97(14). 143114-3.
[188] Gao J-H, Ishida N, Scott I, Fujita D. Controllable growth of single-layer graphene on a Pd(111) substrate. Carbon 2012;50(4):1674–80.
[189] Biris AR, Ardelean S, Lazar MD, Dervishi E, Watanabe F, Ghosh A, et al. Synthesis of few-layer graphene over gold nanoclusters supported on MgO. Carbon 2012;50(6):2252–63.
[190] Chen S, Cai W, Piner RD, Suk JW, Wu Y, Ren Y, et al. Synthesis and characterization of large-area graphene and graphite films on commercial Cu–Ni alloy foils. Nano Lett 2011;11(9):3519–25.
[191] Liu X, Fu L, Liu N, Gao T, Zhang Y, Liao L, et al. Segregation growth of graphene on Cu–Ni alloy for precise layer control. J Phys Chem C 2011;115(24):11976–82.
[192] Liao C-D, Lu Y-Y, Tamalampudi SR, Cheng H-C, Chen Y-T. Chemical vapor deposition synthesis and Raman spectroscopic characterization of large-area graphene sheets. J Phys Chem A 2013;117(39):9454–61.
[193] Memon NK, Kear BH, Tse SD. Transition between graphene-film and carbon-nanotube growth on Nickel alloys in open-atmosphere flame synthesis. Chem Phys Lett 2013;570:90–4.
[194] Wu Y, Chou H, Ji H, Wu Q, Chen S, Jiang W, et al. Growth mechanism and controlled synthesis of AB-stacked bilayer graphene on Cu-Ni alloy foils. ACS Nano 2012;6(9):7731–8.
[195] Yuan S, Meng L, Wang J. Greatly Improved methane dehydrogenation via Ni adsorbed Cu(100) surface. J Phys Chem C 2013;117(28):14796–803.
[196] Wan D, Lin T, Bi H, Huang F, Xie X, Chen IW, et al. Autonomously controlled homogenous growth of wafer-sized high-quality graphene via a smart Janus substrate. Adv Func Mater 2012;22(5):1033–9.
[197] Dai B, Fu L, Zou Z, Wang M, Xu H, Wang S, et al. Rational design of a binary metal alloy for chemical vapour deposition growth of uniform single-layer graphene. Nat Commun 2011;2:522.
[198] Weatherup RS, Bayer BC, Blume R, Ducati C, Baehtz C, Schlögl R, et al. *In situ* characterization of alloy catalysts for low-temperature graphene growth. Nano Lett 2011;11(10):4154–60.
[199] Lu Z, Deng J, Wang J, Yao N, Zhang B. Controllable growth of graphene by changing the microstructure of Fe–Cr–Ni catalyst. Phys Status Solidi (c) 2011;9(1):62–5.
[200] Wu YA, Fan Y, Speller S, Creeth GL, Sadowski JT, He K, et al. Large single crystals of graphene on melted copper using chemical vapor deposition. ACS Nano 2012;6(6):5010–7.

[201] Gao J-H, Fujita D, Xu M-S, Onishi K, Miyamoto S. Unique synthesis of few-layer graphene films on carbon-doped $Pt_{83}Rh_{17}$ surfaces. ACS Nano 2010;4(2):1026–32.
[202] Siller RH, Oates WA, McLellan RB. The solubility of carbon in palladium and platinum. J Less Common Met 1968;16(1):71–3.
[203] Selman GL, Ellision PJ, Darling AS. Carbon in platinum and palladium- solubility determinations and diffusion at high temperatures. Platinum Met Rev 1970;14(1):14–20.
[204] Vanin M, Mortensen JJ, Kelkkanen AK, Garcia-Lastra JM, Thygesen KS, Jacobsen KW. Graphene on metals: a van der Waals density functional study. Phys Rev B 2010;81(8):081408.
[205] López GA, Mittemeijer EJ. The solubility of C in solid Cu. Scri Materialia 2004;51(1):1–5.
[206] Adamska L, Lin Y, Ross AJ, Batzill M, Oleynik II. Atomic and electronic structure of simple metal/graphene and complex metal/graphene/metal interfaces. Phys Rev B 2012;85(19):195443.
[207] Giovannetti G, Khomyakov PA, Brocks G, Karpan VM, van den Brink J, Kelly PJ. Doping graphene with metal contacts. Phys Rev Lett 2008;101(2):026803.
[208] Hesjedal T. Continuous roll-to-roll growth of graphene films by chemical vapor deposition. Appl Phys Lett 2011;98(13). 133106-3.
[209] Wang Y, Zheng Y, Xu X, Dubuisson E, Bao Q, Lu J, et al. Electrochemical delamination of CVD-grown graphene film: toward the recyclable use of copper catalyst. ACS Nano 2011;5(12):9927–33.
[210] Ding G, Zhu Y, Wang S, Gong Q, Sun L, Wu T, et al. Chemical vapor deposition of graphene on liquid metal catalysts. Carbon 2013;53:321–6.